

Monte Carlo Simulations of Type Ia Supernova Observations in Supernova Surveys

Weidong Li, Alexei V. Filippenko

Department of Astronomy, University of California, Berkeley, CA 94720-3411

and

Adam G. Riess

Space Telescope Science Institute, 3700 San Martin Drive, Baltimore, MD 21218

Received _____; accepted _____

ABSTRACT

We have performed Monte Carlo simulations of type Ia supernova (SN Ia) surveys to quantify their efficiency in discovering peculiar overluminous and underluminous SNe Ia. We determined how the type of survey (magnitude-limited, distance-limited, or a hybrid) and its characteristics (observation frequency and detection limit) affect the discovery of peculiar SNe Ia. We find that there are strong biases against the discovery of peculiar SNe Ia introduced by at least four observational effects: the Malmquist bias, the age of the SN Ia at the time of its discovery, the shape of its light curve, and its degree of extinction. Surveys with low observation frequency (less than once per 10 days) tend to discover SNe Ia which are too old for observers to easily recognize their peculiarity. Subluminous SNe Ia are underrepresented in magnitude-limited surveys because they can only be found within a small volume and they remain above the detection limit for less time. Conversely, overluminous SNe Ia are more easily found in magnitude-limited surveys, although their likely association with dusty regions reduces the volume in which they can be discovered. The unbiased rate of peculiar SNe Ia can be recovered only in distance-limited surveys with high observation frequencies and with detection limits which are fainter than the peak magnitude of a subluminous SN Ia in the farthest potential host.

Subject headings: methods: numerical – supernovae: general

1. Introduction

Since supernovae were first recognized by Baade & Zwicky (1934) as a class of objects distinct from common novae, over 1,600 of them have been discovered by professional and amateur astronomers. A record high of over 200 SNe were discovered in 1999.

Most of the SNe were found during systematic SN searches (also known as SN surveys), the first of which was conducted by Zwicky using the 0.46-m Schmidt telescope at Palomar Observatory (the Palomar SN Survey; Zwicky 1938; Kowal et al. 1974). There have been a number of successful SN surveys in the past, such as the Asiago SN survey (Ciatti & Rosino 1978), the Berkeley Automated SN Search (BASS; Perlmutter et al. 1992), and the Calán/Tololo SN survey (CTSS; Hamuy et al. 1993). Many SNe were also discovered in the course of the first generation and second generation Palomar Observatory Sky Surveys (POSS I & II; e.g., Reid et al. 1991) and the UK Schmidt Sky Survey (e.g., Corwin, de Vaucouleurs, & de Vaucouleurs 1977). The number of active professional SN surveys is currently at an all-time high: the Lick Observatory SN Search (LOSS, Treffers et al. 1997; Li et al. 2000a; Filippenko et al. 2000), the Beijing Astronomical Observatory SN Survey (BAOSS; Li et al. 1996), the Perth Observatory SN Search (Williams et al. 1995), the Nearby Galaxies SN Search (Strolger et al. 1999), the High-Z SN Search (HZSS; e.g., Schmidt et al. 1998), the SN Cosmology Project (SCP; e.g., Perlmutter et al. 1997), the Mount Stromlo Abell Cluster SN Search (MSACSS; Reiss et al. 1998), the Wise Observatory Optical Transients Search (WOOTS; Gal-Yam & Maoz 1998), the EROS experiment (e.g., Palanque-Delabrouille et al. 1998), and others. Amateur astronomers, armed with modern, inexpensive CCD cameras and moderately large telescopes, have contributed significantly to the discoveries of SNe. To name a few, the UK nova/SN patrol (e.g., Hurst & Armstrong 1998), the Tenagra Observatories (Schwartz 1997), and the Puckett Observatory (Puckett 1998) are all quite successful in discovering SNe.

Most of these SN surveys can be described using two categories based on how the survey fields are selected: magnitude-limited and distance-limited. In a magnitude-limited SN survey, the target fields are usually random regions on the sky that contain many galaxies at different redshifts. The number of SNe discovered depends on the detection limit of the images (hence magnitude-limited). The CTSS, HZSS, SCP, and EROS experiment are examples of magnitude-limited SN surveys. In a distance-limited SN survey, in contrast, the target fields are usually individual galaxies or clusters of galaxies. The limiting magnitude of the survey images may be much deeper than all the possible SNe in the sample galaxies at peak (as long as they are not heavily extinguished), so the number of SNe discovered largely depends on the number and distances of the sample galaxies or clusters (hence distance-limited). LOSS, BAOSS, and BASS are examples of distance-limited SN surveys. A few SN surveys, however, are best described as a hybrid of these two categories. For example, MSACSS searches a number of Abell clusters of galaxies with fixed redshifts, but half of the SNe were actually discovered in the background of the clusters and some of them have magnitudes close to the detection limit of the survey images. The SNe

discovered in the target galaxy clusters are distance-limited but the background ones are magnitude-limited.

The discovery and observation of Type Ia SNe (SNe Ia), generally the most luminous and homogeneous SNe, have been increasingly emphasized in modern SN surveys because of their utility for cosmological studies (see Riess et al. 1999a, and references therein). In particular, HZSS, SCP, MSACSS, and WOOTs are all designed to search for SNe Ia. SNe Ia have been used to measure the current expansion rate of the Universe, study the peculiar velocities of distant galaxies as well as the bulk flow of our own local neighborhood, examine the nature of the redshift using the time dilation test, probe the nature of extragalactic dust, study the chemical evolution of galaxies, and measure the expansion history of the Universe.

Although SNe Ia are more homogeneous than other classes of SNe, diversity among them was recognized and has been quantified during the last decade. It is now generally thought that SNe Ia can be subclassified by their spectral characteristics as SN 1991T-like, normal, and SN 1991bg/1986G-like (hereafter SN 1991bg-like) objects (see Filippenko 1997 for a review, and references therein; Leibundgut 2000). Both the SN 1991T-like and the SN 1991bg-like objects are also called “spectroscopically peculiar SNe Ia.” SN 1991T-like objects are peculiar as their spectra do not show the classic Si II 6150 Å line of normal SNe Ia but show strong Fe III lines. SN 1991bg-like objects are peculiar as their spectra show an enhanced Si II 5800 Å absorption and a broad absorption trough extending from about 4100 to 4400 Å (probably due to Ti II lines). Li et al. (2000c) point out the existence of a class of “SN 1999aa-like” objects, which are spectroscopically similar to SN 1991T-like objects but also show apparent Ca II H&K lines that are weak in SN 1991T. Whether those SN 1999aa-like objects are the missing link between SN 1991T-like events and normal SNe Ia remains to be determined. In this paper we do not differentiate between SN 1991T-like and SN 1999aa-like objects, instead calling all of them SN 1991T-like.

The variations among light-curve shapes, luminosity, and spectral evolution of the different major subtypes of SNe Ia introduce several observational biases in SN surveys, which can profoundly affect the observed peculiarity rate and the observed luminosity function of SNe Ia (the number distribution of SNe Ia among the three subtypes). Since the intrinsic peculiarity rate and the true luminosity function of SNe Ia hold important clues to their theoretical models, and since it is important to understand the completeness of different kinds of SN Ia surveys, we have written Monte Carlo codes to study the discovery efficiency of SNe Ia in both the distance-limited and the magnitude-limited SN surveys. The preliminary results of the simulations were reported by Li et al. (2000b), but the final results are described here. These will also be used in a companion paper (Li et al. 2000c), where the intrinsic peculiarity rate and the intrinsic luminosity function of SNe Ia are investigated with the sample of SNe Ia discovered during the course of LOSS and BAOSS. Hamuy & Pinto (1999) have used a similar approach to study the observational biases in CTSS, and we compare our results with theirs.

This paper is organized as follows. Sec. 2 presents the various observational biases for SNe Ia in SN surveys, and Sec. 3 reports the outcomes of the Monte Carlo simulations. We discuss our results in Sec. 4 and summarize our conclusions in Sec. 5.

2. The Observational Biases

The differences among the luminosities, light-curve shapes, and spectroscopic evolution of the three major subtypes of SNe Ia result in four main observational biases in SN surveys: the “age bias,” the Malmquist bias, the “light-curve shape (LCS) bias,” and the “extinction bias.”

2.1. The Age Bias

The spectroscopic peculiarity of SN 1991T-like objects can be easily detected only prior to or near maximum brightness (e.g., Filippenko et al. 1992a; Phillips et al. 1992); thus, we cannot be sure whether the SNe discovered more than a week after maximum are peculiar (SN 1991T-like). If these SNe are counted as normal in the sample, it will underestimate the peculiarity rate and change the luminosity function of SNe Ia.

2.2. The Malmquist Bias

SN 1991T-like objects are intrinsically brighter by ~ 0.4 mag at peak (e.g., Filippenko et al. 1992a; Phillips et al. 1992) and SN 1991bg-like objects are intrinsically fainter by ~ 2 mag (e.g., Filippenko et al. 1992b; Leibundgut et al. 1993) than normal SNe Ia in the B band. The difference in other photometric bands (e.g., V or R) varies and is discussed in more detail in the next section. This difference in the luminosity results in a Malmquist bias that affects the observed peculiarity rate and luminosity function of SNe Ia.

Assume all three kinds of objects suffer equal amounts of extinction. A magnitude-limited supernova survey will then overestimate the rate of SN 1991T-like objects because of the larger volume of space surveyed for such objects. It will also underestimate the rate of SN 1991bg-like objects because of the smaller volume of space surveyed for those objects.

The case for a distance-limited supernova survey is more complicated. Whether the Malmquist bias underestimates or overestimates the rates depends sensitively on the characteristics of the survey such as the limiting distance, the limiting magnitude, and the baseline (the time interval to repeat the observations). More details about the Malmquist bias are addressed in the sections on Monte Carlo simulations.

2.3. The Light-Curve Shape Bias

There is an observational bias caused by the differences among the light-curve shapes of SNe. SN 1991T-like objects rise to their maxima and decline thereafter more slowly than do normal SNe Ia; they have the so-called “slow light curves.” SN 1991bg-like objects rise to their maxima and decline thereafter more quickly than do normal SNe Ia; they have the so-called “fast light curves.” The LCS bias affects the amount of time a SN Ia is above the detection limit and its changing brightness from one epoch to another, and hence the discovery efficiency and the distribution of the epoch of discovery as well. These factors result in an observational bias that affects the observed peculiarity rate and luminosity function of SNe Ia.

2.4. The Extinction Bias

There is evidence that SN 1991T-like objects may suffer more extinction than the other two kinds of objects because they are usually (perhaps always) seen in dusty, star-forming regions. For example, four known SN 1991T-like objects all show a significant amount of reddening $E(B - V)$: SN 1991T has 0.13 mag (Filippenko et al. 1992a), SN 1995ac has 0.17 (Riess et al. 1999a), SN 1995bd has 0.5 (Riess et al. 1999a), and SN 1997br has 0.35 (Li et al. 1999). When the Galactic component of the extinction is subtracted according to the map of Schlegel, Finkbeiner, & Davis (1998), the intrinsic reddening due to the host galaxy of the SN is $E(B - V) = 0.11$ mag for SN 1991T, 0.13 mag for SN 1995ac, 0.00 mag for SN 1995bd, and 0.24 mag for SN 1997br. The mean reddening of these four SN 1991T-like objects is $E(B - V) = 0.12$ mag, higher than the mean host-galaxy reddening of $E(B - V) = 0.05$ mag for 26 normal SNe Ia studied by Phillips et al. (1999). If the three major subtypes of SNe Ia indeed suffer different amounts of extinction, the observed peak apparent magnitude will be affected and an observational bias similar to the Malmquist bias results.

3. The Monte Carlo Simulations

3.1. Assumptions

To study the roles of various observational biases, we have written a Monte Carlo code to simulate magnitude-limited and distance-limited SN surveys. We make a number of assumptions in our study:

- (1) SNe Ia are distributed uniformly in space.
- (2) The absolute magnitude for a normal SN Ia is -19.5 (in the R band; see discussions

below).

(3) We assume that the objects have the R -band light curves shown in Figure 1. We choose to use the R band because most modern CCD SN surveys are done in unfiltered mode, whose closest match to the standard passbands is R . We have constructed the R -band light curve of SN 1991T-like objects from the data of SN 1991T (Lira et al. 1998), SN 1995ac (Riess et al. 1999a), and SN 1998es (Li et al. 2000d). A 6-order cubic spline is used to fit the data of the 3 SNe from -13 days to 80 days. We have used the data of SNe 1998de, 1999by, and 1999da (Li et al. 2000e) to construct the R -band light curve of SN 1991bg-like objects from -11 to 80 days. The R -band light curve of SN 1994ae from -12 to 80 days (Riess et al. 1999a) is adopted as that of the normal objects. The rising parts of the light curves of these SNe are constructed according to the recipe described by Riess et al. (1999b), where we adopted risetimes of 24.0, 21.0, and 18.0 days for SN 1991T-like, normal, and SN 1991bg-like objects, respectively. Those risetimes are their counterparts in the B band (Riess et al. 1999b) plus 2.0, 2.0, and 1.5 days for the SN 1991T-like, normal, and 1991bg-like objects, respectively; observations usually show that the R -band maximum follows the B -band maximum by about 2 days. As the adopted light curves of the SNe play an important role in our simulations, in Sec. 4 we will investigate the results of using light curves in other passbands. Following convention, the time of B maximum brightness is defined as $t = 0$ (or epoch = 0) throughout this paper.

(4) There is 0.35 mag of scatter in the absolute magnitudes of each type of SN Ia in the R band. This scatter is chosen to be similar to that found in the B and V bands for normal SNe Ia (e.g., Hamuy et al. 1996c). In the simulations, the scatter is introduced by changing the magnitude of each SN by a normally distributed number with $1\sigma = 0.35$ mag. Note that this simple luminosity function for normal SNe Ia (a Gaussian distribution with $1\sigma = 0.35$ mag, centered at -19.5 mag) is different from that found by Hamuy & Pinto (1999) for CTSS, which is quite flat from -19.0 to -19.9 . However, since there is no luminosity function available for the SN 1991T-like and SN 1991bg-like objects, we choose to use a Gaussian distribution for all three kinds of objects to be consistent.

(5) We assume that SN 1991T-like objects are intrinsically 0.4 mag brighter, and SN 1991bg-like objects are intrinsically 1.0 mag fainter, than normal SNe Ia in the R band. The peak apparent magnitudes in the B and R bands after correction of extinction are about the same for the SN 1991T-like objects (Lira et al. 1998; Riess et al. 1999a; Li et al. 2000d) and the normal objects (Riess et al. 1999a), so we have adopted their difference of luminosity in the B band (0.4 mag) to be that in the R band. The peak apparent magnitude of SN 1991bg-like objects in the R bands is found to be about 1 mag brighter than that in the B band (Li et al. 2000e), so we derive that they are about 1.0 mag fainter than the normal SNe Ia in the R band if we assume that there is a 2.0 mag difference in the B band.

(6) To study the effects of extra extinction for SN 1991T-like objects (the extinction

bias), we have modeled three cases: (a) they have R -band extinction $A_R = 2.5E(B - V)$ equal to that of the other two kinds of objects [hereafter the case SN 1991T ($A=0$)]; (b) they suffer 0.4 mag more extinction than the other two kinds of objects [hereafter the case SN 1991T ($A=0.4$)]; and (c) they suffer 0.8 mag more extinction than the other two kinds of objects [hereafter the case SN 1991T ($A=0.8$)].

(7) We assume that a SN is detected when its magnitude is brighter than the limiting magnitude of the survey by a small number drawn from the positive part of a normal distribution with $1\sigma = 0.3$ mag. There are several reasons why the SN has to be *brighter than* the limiting magnitude to be discovered: (a) there is extinction in the Galaxy and in the host galaxy of the SN; (b) the weather may not always be good enough for the surveys to reach their limiting magnitudes; (c) SNe often occur in complex regions of the host galaxy, making them difficult to discover at the limiting magnitude. Note that the situation of real observations is often more complicated than our simple model of accounting for extinction, weather, and background. In particular, the extinction to the SN depends on both the Galactic extinction to its host galaxy (which is constant) and the supernova’s relative position within the host (close to spiral arms, etc.), and weather conditions usually have their own patterns. However, since our simulations are not done for a particular survey with known weather patterns, there is no readily available mathematical description of the real situation and we have chosen to do the most general case.

(8) We assume that when a SN 1991T-like object is discovered more than 7 days past maximum brightness, it is not distinguished as a SN 1991T-like object, but rather is classified as a normal SN Ia by the observer because the spectrum looks normal. The cutoff of 7 days past maximum brightness is arbitrary, and is used to demonstrate the effect of the age bias. In the discussion section we will explore the results of the simulations using different cutoffs.

(9) We do not simulate the position of the SN in the host galaxy, which means that the discovered SN does not need to have a minimum projected separation from the galactic nucleus or other regions of high surface brightness like H II regions or spiral arms. This is generally acceptable for CCD SN surveys, except perhaps in the central few arcseconds of galaxies with starlike nuclei, but unacceptable for photographic surveys as discussed by Hamuy & Pinto (1999). We also do not simulate the Hubble types of the host galaxies of the SNe.

(10) We do not take into account practical limitations on telescope time. A supernova survey with a limiting magnitude of 19.0 and a baseline of only one day will need more than the available time per night when there are many fields in the sample. In our simulations, we assume all galaxies can indeed be observed with the desired frequency.

(11) We do not take into account the effect of the seasons. In other words, all the SNe used in the simulations are those *observable* by the observers. In practice, most galaxies will have a long period of time (about 5 months) when they not observable because of their

proximity to the Sun. Since the effect of the seasons is similar to decreasing the input number of all three kinds of SNe proportionally, we do not consider it in our simulations.

(12) We do not consider the effect of the redshift (the “ K -correction”), the time-dilation effect, or the geometry of space. All these effects are negligible in our simulations of nearby SNe Ia.

(13) We do not apply the luminosity vs. light-curve shape correlation (e.g., Phillips et al. 1999; Riess et al. 1998; Perlmutter et al. 1997), beyond simply adopting different average light curves for the three subclasses of SNe Ia. Our simulations are done in the R band, where there is little information for variations within a given subclass.

(14) Generally there is a gap (2 to 5 days, sometimes longer) between the time of a SN discovery and the time of its spectroscopic classification. Since the peculiarities considered here are spectral, it is important to simulate this fact to study the age bias. In the simulations the time of the spectroscopic classification of a SN is taken to be its discovery epoch plus an offset of a random time between 2 and 5 days.

(15) For convenience, we need to choose an initial luminosity function of SNe Ia. In our simulations, we assume that SN 1991bg-like and SN 1991T-like objects have the same number density, and that normal SNe Ia have a number density that is four times higher than either of them. This choice of luminosity function is quite arbitrary and is used only to demonstrate the effects of the various observational biases on the detection efficiency of different kinds of objects (nevertheless, a luminosity function similar to this is found by Li et al. [2000c]). Choosing a different luminosity function will not change the major results of the simulations. In particular, we will evaluate the effects of the observational bias on the SN 1991bg-like objects by considering SN 1991bg-like and normal objects only (which means an input rate of SN 1991bg-like objects of 20%); the same is true for dealing with SN 1991T-like objects. The intrinsic luminosity function of SNe Ia is discussed in the companion paper by Li et al. (2000c).

3.1.1. Magnitude-Limited Supernova Survey

Throughout this paper distances are expressed in terms of the distance modulus (μ_0). The apparent magnitude (m) of a normal SN Ia at a distance modulus μ_0 is $m_{normal} = \mu_0 - 19.5$.

The limiting magnitude of the survey is set to be 19.0. This is an arbitrary choice and the results can be scaled. We use 20,000,000 normal SNe Ia uniformly distributed in space to a distance of $\mu_0 = 39.55$ mag, where a normal SN Ia has an apparent magnitude of 20.05. Because of the scatter of magnitudes, we need to consider distances where normal SNe are fainter than the limiting magnitude. We adopt $\mu_0 = 39.55$ mag because the resulting magnitude for a normal SN Ia (20.05) is the limiting magnitude of 19.0 plus 3σ (1.05 mag)

of the scatter in magnitudes.

Since SN 1991T-like objects are more luminous by 0.4 mag than normal SNe Ia, the survey can detect SN 1991T-like objects to $\mu_0 = 39.95$ mag (where normal SNe Ia reach 20.45 mag) for the case SN 1991T ($A=0$). Thus, the space volume in which SN 1991T-like objects ($A=0$) can be detected is 1.738 times that of the normal SNe Ia. With our adopted number density this means that there are 8,690,000 SN 1991T-like objects observable by the survey.

For the case SN 1991T ($A=0.4$), SN 1991T-like objects have apparent magnitudes that are the same as those of the normal objects. Hence, there are 5,000,000 SN 1991T-like objects observable by the survey. For the case SN 1991T ($A=0.8$), the survey can only detect SN 1991T-like objects to a distance of $\mu_0 = 39.15$ mag (where normal SNe Ia reach 19.65 mag). The space volume in which SN 1991T-like objects can be detected is then only 0.575 times that of the normal SNe Ia, which means that there are 2,875,000 SN 1991T-like objects observable by the survey.

Likewise, the space volume in which SN 1991bg-like objects can be detected is only 0.251 times that of the normal SNe Ia, which means that there are 1,255,000 SN 1991bg-like objects observable by the survey.

All of these SNe are binned into 0.01 mag intervals, and their number distributions are shown in Figure 2. This is the input to the Monte Carlo simulation of the magnitude-limited supernova survey.

Even at the time of the input, the Malmquist bias dramatically changes the observed relative frequencies of peculiarity in some cases. The percentage of peculiar SNe Ia relative to normal objects becomes 5.0% for SN 1991bg-like objects (20% intrinsic); and 30.3% for SN 1991T ($A=0$), 20.0% for SN 1991T ($A=0.4$), and 12.6% for SN 1991T ($A=0.8$) (20% intrinsic).

The only parameter in the simulation of the magnitude-limited survey is the baseline. We have simulated results for baselines $t_b = 1, 3, 5, 7, 10, 15, 20, 25, 30, 40, 50,$ and 60 days. For a given baseline (t_b), a SN in a magnitude bin is given a normally distributed scatter with $1\sigma = 0.35$ mag, and the limiting magnitude of the survey is modified (made brighter) by a number drawn from the positive part of a normal distribution with $1\sigma = 0.3$ mag. The SN is then assigned a random observation time (t_{obs}) between 0.0 and t_b before maximum. With t_b and t_{obs} the simulation goes through the light curve of the SN and finds the brightest point at which the SN would be observed in the series of images $t_{obs}, t_{obs} + t_b, t_{obs} + 2 * t_b, \dots$, to see whether it is brighter than the modified limiting magnitude; if it is, the SN is marked as being detected. The simulation also goes through the light curve of the SN to find the earliest time that the SN could have been discovered (e.g., time series of $t_{obs}, t_{obs} - t_b, t_{obs} - 2 * t_b, \dots$); this is the epoch of discovery for the SN.

The results of our simulation are shown in Figures 3 through 6. Figure 3 illustrates the

number of SNe discovered at different apparent magnitudes. Notice that the dotted lines marked “perfect” in the figure represent the number of SNe versus apparent magnitude at maximum brightness *after* adding Gaussian scatter with $1\sigma = 0.35$ mag, not the input distributions without adding scatter as in Figure 2. Here we emphasize again that each subclass of peculiar SNe Ia is studied by comparing that subclass with the normal subclass only. Figure 3 contains two of the four cases: SN 1991bg-like objects and the case SN 1991T ($A=0$). The upper panel shows the number distribution of the peculiar SNe Ia, while the lower panel shows the corresponding number distribution of the normal SNe. The other two cases [SN 1991T ($A=0.4$) and SN 1991T ($A=0.8$)] are not shown, but their results are similar to the case SN 1991T ($A=0$).

We notice the following. (1) Even with a baseline of only one day, not all SNe can be discovered, and the fainter the apparent magnitude, the more the SNe are lost in the survey. The discovery efficiency (the number of SNe discovered divided by the input number of SNe with $\text{mag} \leq 19.0$; see Figure 4) can only reach a maximum of 84% for all three kinds of objects. (2) The longer the baseline, the more SNe are lost in the survey. (3) For the case SN 1991T ($A=0$), when the baseline is 30 days, the number of normal SNe detected with apparent magnitude brighter than about 18 is slightly more than the number of normal SNe Ia at that magnitude on the “perfect” line. This is caused by the fact that with such long baselines, some SN 1991T-like objects are discovered later than one week past maximum and are counted as normal SNe Ia due to the age bias.

Figure 4 shows the discovery efficiency at different baselines. The upper two panels display the results of the SN 1991bg-like and the SN 1991T-like objects, while the bottom panel shows the result of SN 1991T-like objects without considering the age bias. Things to notice are as follows. (1) The discovery efficiency declines quickly with increasing baselines. (2) In the middle panel, all three cases ($A=0$, $A=0.4$, and $A=0.8$) have the same discovery efficiency for the SN 1991T-like objects, but the corresponding normal objects have different discovery efficiencies at long baselines. This is caused by the fact that when the extinction is bigger, there are fewer SN 1991T-like objects observable by the survey; consequently, there are fewer SN 1991T-like objects discovered later than a week past maximum and counted as normal. The case SN 1991T ($A=0.4$) (the dashed line) thus has a smaller discovery efficiency for the normal objects, while the case SN 1991T ($A=0.8$) (the dotted line) has the smallest. (3) When the baseline is shorter than 10 days, the normal objects have a larger discovery efficiency than the SN 1991bg-like objects, but the SN 1991T-like objects have a slightly larger discovery efficiency than the normal objects. The main reason for this is the different light-curve shapes. Among the three kinds of SNe Ia, the SN 1991T-like objects spend the longest time bright because of their broad light curves, and thus have the largest discovery efficiency. (4) When the baseline is longer than 10 days, however, the normal SNe Ia have a larger discovery efficiency than the SN 1991T-like objects. The main reason for this is the fast decline of the discovery efficiency of the SN 1991T-like objects, which results from the age bias; some of the SN 1991T-like objects are discovered later than a

week past maximum and are counted as normal SNe Ia. If we do not consider the age bias in the simulations as shown in the bottom panel, the SN 1991T-like objects have a larger discovery efficiency at all baselines.

Figure 5 shows the distribution of the epoch of discovery in the simulations, where the epoch of maximum brightness is day 0. The case for SN 1991bg-like objects and the case SN 1991T ($A=0$) are displayed. Again, the corresponding distributions for the normal SNe are shown in the lower panel. We see the following. (1) The smaller the baseline, the earlier is the peak in the discovery epoch. The epoch of discovery peaks at about -6 , -11 , and -12 days for the SN 1991bg-like, normal, and SN 1991T-like objects, respectively, when the baseline is 1 day, and this changes to -2 , -4 , -6 days when the baseline is 10 days. (2) The majority of SNe Ia can be detected before maximum only when the baseline of the survey is smaller than 10 days. (3) For the SN 1991T-like objects, the distribution has a gradual cutoff from $+2$ to $+5$ days when the baseline is longer than 30 days because of the age bias. Since the cutoff of the age bias is $+7$ days, and there is a random gap of 2 to 5 days between the epoch of discovery and the time of spectroscopic classification, the discovery epoch of SN 1991T-like objects should have this gradual cutoff from $+2$ to $+5$ days, and no SN 1991T-like objects should be identified by the observer when their discovery epoch is later than $+5$ days. (4) The distribution of normal SNe Ia has a gradual increase from $+2$ to $+5$ days and forms a second peak for the same reason. (5) For a given baseline, the SN 1991bg-like objects have the narrowest peak in the distribution, and the SN 1991T-like objects have the broadest peak. This is caused by the difference in the light-curve shapes. The SN 1991bg-like objects have the narrowest light curve, so the detected events have the largest probability of being discovered near maximum brightness, while the SN 1991T-like objects have the broadest light curve, so the detected events spread out in the epoch of discovery.

Figure 6 shows the observed peculiarity rates in our simulations. The input rate for each type of SN is shown as dash-dotted lines. The difference between the output peculiarity rates and their input values also reflects the relative change in the luminosity function. We see the following. (1) The magnitude-limited surveys significantly underestimate the rate of SN 1991bg-like objects for all baselines. The rate changes from 20.0% (the input peculiarity rate) to about 5.5%. (2) For the case SN 1991T ($A=0$), the surveys overestimate the rate of SN 1991T-like objects when the baseline is smaller than 35 days, but underestimate it with larger baselines. The rate changes from 20.0% to more than 30% at small baselines. The rate of SN 1991T-like objects first becomes larger with increasing baseline, because SN 1991T-like objects are easier to discover due to their broader light curves; it subsequently declines quickly with increasing baselines because of the age bias. (3) For the case SN 1991T ($A=0.4$), SN 1991T-like objects have the same luminosities as the normal objects, yet their rate is slightly larger than the input value when the baseline is small because of the LCS bias, and is smaller than the input value when the baseline is large because of the age bias. (4) For the case SN 1991T ($A=0.8$), the surveys underestimate the rate of SN

1991T-like objects at all baselines (smaller than 14%). The rate of SN 1991T-like objects is less than 10% when the baseline is longer than 30 days.

3.1.2. Distance-Limited Supernova Survey

We assume the limiting distance is where normal SNe Ia have an apparent magnitude at maximum of 16.0 ($\mu_0 = 35.5$, ~ 130 Mpc), and there are 4,000,000 normal SNe Ia in that volume (down to mag 16.0). With our arbitrary luminosity function for SNe Ia, there are 1,000,000 SN 1991T-like objects in the sample with magnitude down to 15.6, 16.0, or 16.4 for the case SN 1991T ($A=0.0$), ($A=0.4$), or ($A=0.8$), respectively, and there are 1,000,000 SN 1991bg-like objects with magnitude down to 17.0. All the SNe are binned into 0.01 mag intervals, and their number distributions are shown in Figure 7.

There are two parameters for the distance-limited survey: the limiting magnitude of the survey and the baseline. We have simulated results for limiting magnitudes of 15.0, 15.5, 16.0, 16.5, 17.0, 17.5, 18.0, 18.5, and 19.0. The choice of baseline is the same as for the magnitude-limited SN survey: 1, 3, 5, 7, 10, 15, 20, 25, 30, 40, 50, and 60 days. The method of the simulations is basically the same as we described in the magnitude-limited SN survey, the only difference being that the limiting magnitude is now a changing parameter.

Some of the results of the simulations are displayed in Figures 8 through 11. Figure 8 shows the number of SNe discovered at different apparent peak magnitudes for surveys with different limiting magnitudes. For each limiting magnitude, results of different baselines are displayed. The results of the case SN 1991T ($A=0.8$) are shown here and the other cases yield similar results.

Inspection of the figure reveals the following.

(1) When the limiting magnitude of the survey is small (bright), such as 15.0, the results of the distance-limited survey are exactly the same as those of a magnitude-limited survey. In fact, for the input parameters of our distance-limited survey, it will behave as a magnitude-limited survey as long as the limiting magnitude of the survey is ≤ 15.6 , the faintest SN 1991T-like objects in the sample for the case SN 1991T ($A=0$).

(2) When the limiting magnitude equals 18.0 or 19.0, the number distributions of the distance-limited survey become different from those of the magnitude-limited surveys. With a small baseline (1 to 10 days), all the SN 1991T-like objects and the normal SNe Ia are discovered in the survey. When the baseline is large (e.g., 30 or 60 days), however, some of the SNe are still lost in the survey.

Figure 9 shows the discovery efficiencies for all cases. In each case results for different baselines and limiting magnitudes are given. Rates for peculiar SNe Ia are in the upper panel, and the corresponding rates for normal SNe Ia are in the lower panel. We notice the

following.

(1) The discovery efficiency generally increases with increasing limiting magnitude. For example, when the baseline equals 20 days, the discovery efficiency for the SN 1991bg-like objects is only about 15% for a limiting magnitude of 16.0, but it becomes 56%, 97%, and 100% for limiting magnitudes of 17.0, 18.0, and 19.0, respectively.

(2) For the SN 1991bg-like objects, the survey discovers all the SNe when the limiting magnitude is 19.0 and the baseline is smaller than 30 days. The discovery efficiency then declines with increasing baselines. For the other limiting magnitudes, the discovery efficiency is always smaller than 1 and declines with increasing baselines.

(3) For the case SN 1991T ($A=0$), the survey discovers all the SNe when the baseline is small enough and the limiting magnitude is fainter than all the SNe in the sample. For example, when the limiting magnitude is 17.5, all SNe are discovered if the baseline is shorter than 20 days. When the baseline becomes longer than that, the efficiency of SN 1991T-like objects declines rapidly, while the corresponding efficiency of normal SNe Ia first rises to above 100%. This is caused by the age bias because some of the SN 1991T-like objects are classified as normal SNe Ia with such long baselines.

(4) Extinction of SN 1991T-like objects seems to play a negligible role in determining the discovery efficiency when the survey has a deep limiting magnitude (e.g., 17.5 and 19.0 in Figure 9) and a small baseline, because all SNe are discovered regardless of the adopted value for the extinction of SN 1991T-like objects. It only affects the survey with a limiting magnitude that is comparable to or brighter than the faintest SNe in the sample (e.g., 16.0 in Figure 9), or when the baseline is long (e.g., > 30 days).

Figure 10 shows the distribution of the epoch of discovery for the case SN 1991T ($A=0.8$). Other cases have similar results. When the baseline is small, such as 5 days, all the distributions exhibit a Gaussian profile except the case of the SN 1991T-like objects with limiting magnitude of 19.0, and the peak shifts toward later epoch of discovery with decreasing limiting magnitudes. When the baseline gets longer, the distribution becomes wider, and begins to show a flat-topped feature. The gradual increase for the normal SNe Ia and cutoff for the SN 1991T-like objects at an epoch of +2 to +5 days when the baseline is 30 or 60 days is caused by the age bias, as discussed previously. The distance-limited surveys with a baseline of 60 days and limiting magnitudes of 18.0 or 19.0 are the only ones that have significant number distributions (e.g., the lower left panel of Figure 10) at a discovery epoch of 20 to 40 days in our simulations.

Figure 11 shows the peculiarity rates from our simulations of the distance-limited surveys. The difference between the output peculiarity rates and their input values also reflects the relative change in the luminosity function. We find the following.

(1) When the limiting magnitude of the survey is bright, such as 15.0, all cases show a rate distribution that is exactly the same as that of the magnitude-limited survey case

(Figure 6). This is because when the limiting magnitude is so bright, the survey is actually limited by its limiting magnitude rather than by the distances of the sample galaxies, so the survey behaves as a magnitude-limited one. This kind of survey seriously underestimates the rate of SN 1991bg-like objects, overestimates the rate of SN 1991T-like objects for the case SN 1991T ($A=0$), overestimates or underestimates the rate of SN 1991T-like objects for the case SN 1991T ($A=0.4$) depending on the baseline of the survey, and underestimates the rate of SN 1991T-like objects for the case SN 1991T ($A=0.8$).

(2) When the limiting magnitude of the survey is 17.0, things become more complicated. For SN 1991bg-like objects, there are many SNe with magnitude fainter than 17.0, so the rate should be the same as that of the magnitude-limited case. Inspection of Figure 11 reveals, however, that this is not the case. The rate for SN 1991bg-like objects is always higher than in the corresponding magnitude-limited case. The reason for this is that we calculate the rate of SN 1991bg-like objects by comparing them with the normal SNe Ia, which are not magnitude-limited (recall that all normal SNe Ia are brighter than mag 16.0). The number of normal objects discovered will always be smaller than in the magnitude-limited case (which have normal SNe Ia observable to mag 17.0), resulting in a higher rate for SN 1991bg-like objects. The cases of SN 1991T ($A=0$) and ($A=0.8$) have similar rate distributions. The rate equals the input value when the baseline is small, and declines with increasing baselines. The extinction seems to only affect the cutoff of the baseline where the observed rate begins to decline from the input value: 20 days for the $A=0$ case and 15 days for the $A=0.4$ case. The SN 1991T ($A=0.8$) case has a rate distribution similar to that of the other SN 1991T cases, but its rate is always smaller than the input one.

(3) When the limiting magnitude of the survey reaches 19.0, a magnitude that is fainter than all the possible SNe in the sample galaxies, all cases show similar rate distributions. The rate is equal to the input value when the baseline is small, but declines with increasing baselines. In particular, when the baseline is smaller than 20 days, the rates for both SN 1991bg-like objects and SN 1991T-like objects equal the input values, regardless of the extinction adopted for SN 1991T-like objects.

4. Discussion

Throughout this paper we have categorized SN 1991T-like and SN 1991bg-like objects as “peculiar” SNe Ia, for historical reasons: those objects were considered rare until a few years ago, and they show distinct spectral features. There are discussions of models for these “peculiar” SNe Ia and whether they represent physically distinct classes of SNe Ia having different explosion mechanism and/or progenitor mass and configuration (e.g., Filippenko et al. 1992a, 1992b; Phillips et al. 1992; Ruiz-Lapuente et al. 1992; Jeffery et al. 1992; Leibundgut et al. 1993; Mazzali et al. 1995; Turatto et al. 1996; Mazzali

et al. 1997), but there is no consensus on the issue yet. It is also still an open question whether SN 1991T-like and SN 1991bg-like objects are part of a spectroscopic and/or photometric sequence, or constitute distinct observational classes. We thus emphasize that we subclassify SNe Ia as SN 1991T-like, normal, or SN 1991bg-like based only upon their *apparent spectroscopic abnormality*; we do not imply that they represent fundamentally different (but related) kinds of objects.

It is also worth pointing out that after finding a high percentage (36%) of SN 1991T-like and SN 1991bg-like SNe Ia (Li et al. 2000c), it becomes questionable whether to categorize these objects as “peculiar.” The classification (normal or peculiar) of SN 1999aa-like objects, which comprised a significant portion of the SN 1991T-like objects in the sample of Li et al. (2000c), also plays an important role. More detailed studies, both observational and theoretical, are needed to address these issues.

In our simulations we have employed a single light-curve shape for each of the three subclasses of SNe Ia. One implication of this assumption is that SN 1991T-like objects always have slower light curves than normal objects, which conflicts with the observations of SN 1992bc (Maza et al. 1994), a normal SN Ia having a slow light curve ($\Delta m_{15}(B) = 0.87$). Hamuy (2000, private communication) also notes that SN 1999ee is a normal SN Ia with a slow light curve. While the frequency of this kind of normal SN Ia remains to be determined, it seems that the correlation between light-curve shape and spectroscopic behavior is not monotonic; two or more parameters may be needed to describe the whole class of SNe Ia. Note, however, that the luminosity difference we adopted for the SN 1991T-like and the normal objects (0.4 mag) is only slightly larger than the assumed 1σ scatter (0.35 mag), which means that some objects overlap in luminosity between the two subclasses. If we had adopted the luminosity vs. light-curve shape relation in our simulations, there would have been some normal SNe Ia having large luminosity and thus having slow light curves. Not doing this is therefore an apparent limitation of our simulations.

In the subsequent sections, we discuss the results of our simulations in the B band, more studies of the age bias, and comparisons of our results with observations.

4.1. The Results of the Simulations in the B Band

Although most modern surveys of nearby SNe are done in unfiltered mode, for which our simulations using the R band should represent the closest match, some surveys are done in other passbands. For example, CTSS was done in the B band with photographic plates, and the SN surveys at high redshift are also done at the rest-frame B band. To investigate the effect of adopting different passbands, we have also done our simulations of magnitude-limited SN surveys in the B band as both CTSS and the high-redshift SN surveys are magnitude-limited (see Sec. 1).

The two major differences of the input to the Monte Carlo simulations of using the B band are as follows. (1) The light curves of the SNe in the B band are different. We have used the B -band light curves shown in Figure 12, where we adopted the data of SN 1991T and SN 1991bg from Hamuy et al. (1996a), and the data of the normal SN 1992al (Hamuy et al. 1996a). The rising parts of the light curves are again constructed according to the recipe described by Riess et al. (1999b), where we adopted risetimes of 22.0, 19.5, and 16.5 days for SN 1991T-like, normal, and SN 1991bg-like objects, respectively. (2) The differences among the luminosities of SNe Ia are different. In the B band, SN 1991T-like objects are 0.4 mag brighter, and SN 1991bg-like objects are 2.0 mag fainter, than normal SNe Ia. The difference of the adopted luminosities changes the input number of SNe to the simulations.

The results of the simulations in the B band are similar, but with subtle differences, to those in the R band in terms of the apparent magnitude distribution (Figure 3), the discovery efficiency at different baselines (Figure 4), and the distribution of the epoch of discovery (Figure 5). The major difference, however, is in the rates as shown in Figure 13. The SN surveys in the B band underestimate the rate of SN 1991bg-like objects more significantly than do those in the R band.

The rate of SN 1991T-like objects shows some interesting differences. Since we have adopted equal luminosities for the SN 1991T-like and the normal SNe Ia in the R and B bands, these differences in the observed rates are mostly caused by the different LCS and age biases. When the baseline is small ($\lesssim 10$ days), both the age bias and the LCS bias are small, so the surveys in the two passbands have the same peculiarity rate for the SN 1991T-like objects. When the baseline is moderately large ($10 \text{ days} < \text{baseline} \leq 33 \text{ days}$), the surveys in the R band have larger rates for the SN 1991T-like objects. The main reason for this is because at such baselines, the broader light curves of SN 1991T-like objects in the R band result in a relatively higher discovery efficiency for them, and yet the age bias is not very severe at these baselines. When the baseline is very large ($> 33 \text{ days}$), the surveys in the B band have higher rates for the SN 1991T-like objects because of the more severe age bias in the SN surveys in the R band. This results from the fact that the R -band light curve is broader than the B -band light curve, so a higher percentage of SNe Ia are discovered later than a week past maximum in the R -band surveys.

4.2. More About the Age Bias

We have used a cutoff of 7 days past peak brightness to simulate the age bias. For such a cutoff we noticed that the age bias has negligible effects in magnitude-limited SN surveys (Figure 6) and distance-limited SN surveys (Figure 11) when the baseline of the surveys is less than 10 days, especially compared to the Malmquist and the LCS biases. This is reasonable since with such small baselines, very few SN 1991T-like objects are discovered

later than a week past maximum and classified as normal.

We have also done simulations with different cutoffs (5, 3, 1, -1 days after peak brightness) to study the age bias, but the results are not shown in Figures 3 through 6 and 8 through 11 because of the increased complexity, making them too difficult to read. Using different cutoffs for the age bias significantly affects the results of the simulations because of the changes in the number of SN 1991T-like objects classified by the observer as normal. The results for the SN 1991bg-like objects are not affected because they are not related to the SN 1991T-like objects. The discovery efficiency of both the SN 1991T-like and the normal objects is affected and the number distribution of SNe versus the epoch of discovery changes according to the adopted cutoffs. The most important changes, however, are those for the rates of SN 1991T-like objects.

Figure 14 shows the rates of SN 1991T-like objects with different cutoffs for the age bias for the magnitude-limited surveys simulated in the B band. The rates of SN 1991T-like objects change dramatically with the different adopted cutoffs – the earlier the cutoff, the smaller the rate of SN 1991T-like objects. For example, for the case SN 1991T ($A=0.4$) with a baseline of 20 days, the rate of SN 1991T-like objects reduces from 16% to 11% to 6%, when the cutoff changes from 7 to 3 to -1 days after peak brightness. The rate of SN 1991T-like objects is only 4% for the case SN 1991T ($A=0.8$) when the adopted cutoff for the age bias is -1 day after (i.e., 1 day before) peak brightness.

Figure 15 shows similar results for the distance-limited surveys simulated in the R band. We notice that when the limiting magnitude is deep enough and the baseline is small enough (e.g., baseline ≤ 10 days for the limiting magnitude 19.0 cases, and baseline ≤ 5 days for the limiting magnitude 17.0 cases except the case with $A=0.8$), the rate of SN 1991T-like objects is still equal to the intrinsic value, regardless of the adopted (reasonable) cutoff and extinction. The reason for this is that in those cases, all SN 1991T-like objects are discovered prior to 1 day before peak brightness, so the observed luminosity function is not affected by the selected cutoff for the age bias or by the adopted extinction. When the baseline becomes larger, however, the earlier the adopted cutoff for the age bias, the smaller the rate of SN 1991T-like objects. When the limiting magnitude of the survey is bright (e.g., the mag 15.0 cases in Figure 15), the survey is actually magnitude-limited as discussed earlier, and the results reflect this for the magnitude-limited surveys in the R band. Comparison with Figure 14 reveals that they are very similar.

As the cutoff of the age bias significantly affects the results of the simulations, we have tried to constrain it from observations. Unfortunately, there are no spectroscopic observations of SN 1991T in the literature between -3 and $+9$ days (e.g., Filippenko et al. 1992a; Phillips et al. 1992a; Ruiz-Lapuente et al. 1992), nor are there any observations of SN 1997br, another SN 1991T-like object (Li et al. 1999), between -4 and $+8$ days. We can see that the spectra of the two objects are very different from those of normal SNe Ia at -3 or -4 days, so the cutoff must be later than -3 days. Their spectra are relatively

similar to those of normal SNe Ia after 8 days, so the cutoff probably should be earlier than 8 days. (Notice that SNe 1991T and 1997br are slightly different from normal SNe Ia at late times, as discussed by Filippenko et al. [1992a] and Li et al. [1999], but these differences are subtle and the spectra do not show the defining features of SN 1991T-like objects – strong Fe III lines and no/weak Si II 6150 Å). This range for the cutoff (–2 to 7 days) is large and does not provide much of a constraint for useful discussions. Li et al. (2000c) compared the spectra of three SN 1999aa-like objects near maximum to those of normal SNe Ia, and suggested that the cutoff of the age bias might be as early as the day of peak brightness or perhaps 1 day earlier. This suggestion, however, depends on whether SN 1999aa-like objects should be considered in the SN 1991T subclass or as “normal” SNe Ia. Further studies of SN 1999aa-like objects and their implications for spectral classification of SNe Ia are needed (e.g., Li et al. 2000d).

As the database of SN Ia spectra becomes better, peculiar ones will become easier to identify. For example, we may not even need the defining characteristics (Fe III lines and no/weak Si II 6150 Å) to identify a SN 1991T-like object. Thus, the age bias will decrease with the observer’s increasing ability to identify peculiarities in the spectrum.

4.3. Comparisons with Observations

Our simulations in the R band indicate that a distance-limited survey with a deep limiting magnitude and a small baseline, such as LOSS and BAOSS (Li et al. 2000c), will discover all the SNe Ia in the sample without any bias against any peculiar types of SNe. The uncertain determination of quantities such as the extra extinction of SN 1991T-like objects and the cutoff of the age bias also plays a negligible role. Li et al. derive the intrinsic peculiarity rate and luminosity function of SNe Ia from 45 SNe Ia discovered in the course of LOSS and BAOSS. They find a high rate for peculiar SNe Ia (about 36%), and that the luminosity function of SNe Ia has 20% SN 1991T-like, 64% normal, and 16% SN 1991bg-like objects.

It is also interesting to compare the results of our simulations with those of real SN surveys. Figure 16 compares the distribution of the epoch of discovery from our simulations with those from LOSS+BAOSS and from CTSS. As indicated by Li et al. (2000c), LOSS and BAOSS are done in the unfiltered mode and are distance-limited surveys with a limiting magnitude of 19.0 and a baseline of ≤ 10 days, and the limiting distance of the sample galaxies is very similar to what we used in our simulations (where normal SNe Ia have a peak apparent magnitude of 16.0). CTSS is done in the B band and is a magnitude-limited survey with a baseline of about 20 days (Hamuy & Pinto 1999). Figure 16 shows that the results of the real SN surveys are quite consistent with those of our simulations.

Hamuy & Pinto (1999) have used the same approach (that is, Monte Carlo simulations) to study the observational biases in CTSS. They simulated the survey as magnitude-limited,

and took into consideration the LCS bias and the Malmquist bias. They also considered the Shaw (1979) effect, which requires the discovered SN to have a minimum projected separation from the nucleus of the host galaxy and is an important observational bias in photographic searches such as CTSS. They used the real observation history of the survey to do the simulation, and a luminosity function of SNe Ia based on the decline rate [that is, L vs. $\Delta m_{15}(B)$]. The age bias, however, was not considered in their simulations. They estimated the degree of incompleteness of the survey as a function of decline rate, and corrected the luminosity function of SNe Ia. They found that the true luminosity function of SNe Ia is remarkably flat over the whole range of decline rates, with perhaps an increase in frequency for the intrinsically faint events.

Adopting the luminosity function of SNe Ia as derived by Li et al. (2000c) and applying the results from our simulations, we find that for a magnitude-limited SN survey in the B band with a baseline of 20 days, SN 1991bg-like and SN 1991T-like objects should comprise about 1% and 27% of the total sample, respectively (assuming SN 1991T-like objects do not suffer more extinction than the other SNe Ia, and adopting a cutoff of 7 days after peak brightness for the age bias). This means that for the 31 SNe discovered in CTSS, there should be 0.3 ± 0.5 SN 1991bg-like objects and 8.4 ± 2.9 SN 1991T-like objects (the uncertainties are derived from Poisson statistics). It is natural that there is one SN 1991bg-like object in the Calán/Tololo sample (SN 1992K; Hamuy et al. 1994), but the fact that no objects were classified as SN 1991T-like is somewhat surprising.

There are several possible reasons for the apparent lack of SN 1991T-like objects. (1) As discussed earlier, they seem more likely to occur in dusty, star-forming regions than the other two kinds of SNe Ia. This causes two difficulties for discovering SN 1991T-like objects in CTSS. First, the star-forming regions are more likely to be overexposed in the photographic plates, resulting in an effect similar to that of Shaw (1979). Second, the dusty environment of SN 1991T-like objects causes them to be more extinguished on average. (2) As also previously discussed, a more serious age bias (e.g., a cutoff of 1 day before peak brightness) significantly reduces the apparent rate of SN 1991T-like objects. The rate of SN 1991T-like objects changes to only 6% and 4% for the cases SN 1991T ($A=0.4$) and SN 1991T ($A=0.8$), which means there should be 1.9 ± 1.4 and 1.2 ± 1.1 SN 1991T-like objects in CTSS, respectively. The statistical significance of the null discovery of SN 1991T-like objects in CTSS thus depends on the still uncertain cutoff of the age bias, but we believe this is the main bias affecting CTSS.

5. Conclusions

The differences among the luminosities, light-curve shapes, and spectroscopic evolution of the three major subtypes of SNe Ia (SN 1991T-like, normal, and SN 1991bg-like) result in several observational biases in SN surveys: the age bias, the Malmquist bias, the light-curve

shape bias, and the extinction bias. These biases affect the observed peculiarity rate and luminosity function of SNe Ia. Under a number of assumptions, we have conducted Monte Carlo simulations of the observations of SNe Ia in the R band in magnitude-limited and distance-limited SN surveys to study the effect of the biases and to investigate the properties of the surveys having different parameters.

We have simulated magnitude-limited SN surveys with a limiting magnitude of 19.0 and a baseline of 1 to 60 days. We find that with our assumptions, the SN discovery efficiency can only reach a maximum of about 84%, and the longer the baseline, the more the SNe are lost and the more serious is the age bias. We also find that the majority of SNe Ia could be detected before maximum brightness only when the baseline of the surveys is $\lesssim 10$ days. We find that the magnitude-limited surveys significantly underestimate the rate of SN 1991bg-like objects, and that the adopted extra extinction for SN 1991T-like objects plays an important role in determining their rate. The surveys overestimate the rate of SN 1991T-like objects if no extra extinction is assumed for them, and underestimate their rate if the adopted extra extinction is larger than 0.4 mag.

We have also simulated distance-limited surveys with a limiting distance where normal SNe Ia have a peak apparent magnitude of 16.0. Results for surveys with limiting magnitude from 15.0 to 19.0 and baseline from 1 to 60 days have been obtained. We find that the discovery efficiency increases with increasing limiting magnitude, and when the limiting magnitude is faint enough (e.g., 19.0) and the baseline is short enough (e.g., $\lesssim 10$ days), all SNe Ia are discovered in a survey. This means that the observed peculiarity rate and luminosity function of SNe Ia in such surveys will be the intrinsic ones. The roles of the LCS bias and the age bias become more important when the baseline is longer and the limiting magnitude is brighter.

It is worth mentioning that although magnitude-limited surveys can bias significantly the luminosity function of SNe Ia, a carefully selected subsample of SNe Ia found in a magnitude-limited survey can actually obey the rules of a distance-limited survey, and thus can produce an unbiased luminosity function of SNe Ia if the baseline of the survey is small enough.

We have done the simulations in the B band and find that these SN surveys underestimate the SN 1991bg-like objects more significantly than do those in the R band. The LCS bias and the age bias for the SN 1991T-like objects are also different in the two passbands, resulting in a different dependence of their peculiarity rate on baselines. We find that the rate of SN 1991T-like objects in the simulations is significantly affected by the adopted cutoff for the age bias. The distance-limited SN surveys with deep limiting magnitude and short baseline remain the best ones for determining the intrinsic peculiarity rate and luminosity function of SNe Ia, as these quantities are not affected by the poorly constrained extra extinction of the SN 1991T-like objects or by the adopted cutoff of the age bias.

We have compared the distribution of the epoch of discovery from our simulations with those of real SN surveys, specifically LOSS+BAOSS and CTSS, and find that they are quite consistent. We have also compared our simulations to those done by Hamuy & Pinto (1999). The lack of SN 1991T-like objects in CTSS is somewhat mysterious, and may be caused by the Shaw effect, extra extinction to such objects, and perhaps most importantly the age bias.

The authors thank the referee, M. Hamuy, for his very helpful comments on the paper. We also thank P. Pinto and M. M. Phillips for many useful discussions. This work is supported by NSF grants AST-9417213 and AST-9987438, as well as by NASA grant AR-08006 from the Space Telescope Science Institute, which is operated by AURA, Inc., under NASA contract NAS5-26555. We are also grateful to the Sylvia and Jim Katzman Foundation for generous donations that made LOSS and the resulting analysis possible.

REFERENCES

- Baade, W., & Zwicky, F. 1934, Proc. Natl. Acad. Sci., 20, 254
- Ciatti, F., & Rosino, L. 1978, Astron. Astrophys. Suppl., 34, 387
- Corwin, H. G., Jr., de Vaucouleurs, A., & de Vaucouleurs, G. 1977, AJ, 82, 557
- Filippenko, A. V. 1997, ARAA, 35, 309
- Filippenko, A. V., et al. 1992a, ApJ, 384, L15
- Filippenko, A. V., et al. 1992b, AJ, 104, 1543
- Filippenko, A. V., et al. 2000, in preparation
- Gal-Yam, A., & Maoz, D. 1998, IAU Circ. 7055
- Hamuy, M., et al. 1993, AJ, 106, 2392
- Hamuy, M., et al. 1994, AJ, 108, 2226
- Hamuy, M., et al. 1996a, AJ, 112, 2438
- Hamuy, M., et al. 1996b, AJ, 112, 2408
- Hamuy, M., et al. 1996c, AJ, 112, 2398
- Hamuy, M., & Pinto, P. A. 1999, AJ, 117, 1185
- Hurst, G. M., & Armstrong, M. 1998, IAU Circ. 6841
- Jeffery, D. J., et al. 1992, ApJ, 397, 304
- Kowal, C. T., et al. 1974, PASP, 86, 516
- Leibundgut, B. 2000, A&A, in press
- Leibundgut, B., et al. 1993, AJ, 105, 301
- Li, W. D., et al. 1996, IAU Circ. 6379
- Li, W. D., et al., 1999, AJ, 117, 2709
- Li, W. D., et al. 2000a, in Cosmic Explosions, eds. S. S. Holt & W. W. Zhang (New York: American Institute of Physics), 103
- Li, W. D., et al. 2000b, in Cosmic Explosions, eds. S. S. Holt & W. W. Zhang (New York: American Institute of Physics), 91

- Li, W. D., et al. 2000c, ApJ, submitted
- Li, W. D., et al. 2000d, in preparation
- Li, W. D., et al. 2000e, in preparation
- Maza, J., et al. 1994, ApJ, 424, L107
- Mazzali, P. A., et al. 1995, A&A, 297, 509
- Mazzali, P. A., et al. 1997, MNRAS, 284, 151
- Palanque-Delabrouille, N., et al. 1998, A&A, 332, 1
- Perlmutter, S., et al. 1992, in *Robotic Telescopes in the 1990s*, ed. A. V. Filippenko (San Francisco: Astron. Soc. Pacific), 67
- Perlmutter, S., et al. 1997, ApJ, 483, 565
- Phillips, M. M., et al. 1992, AJ, 103, 1632
- Phillips, M. M., et al. 1999, AJ, 118, 1766
- Puckett, T. 1998, IAU Circ. 6957
- Reid, I. N., et al. 1991, PASP, 103, 661
- Reiss, D. J., et al. 1998, AJ, 115, 26
- Riess, A. G., et al. 1998, AJ, 116, 1009
- Riess, A. G., et al. 1999a, AJ, 117, 707
- Riess, A. G., et al. 1999b, AJ, 118, 2675
- Ruiz-Lapuente, P., et al. 1992, ApJ, 387, L33
- Schlegel, D. J., Finkbeiner, D. P., & Davis, M. 1998, ApJ, 500, 525
- Schmidt, B. P., et al. 1998, ApJ, 507, 46
- Schwartz, M. 1997, IAU Circ. 6700
- Shaw, R. L. 1979, A&A, 76, 188
- Strolger, L. G., et al., IAU Circ. 7125
- Treffers, R. R., et al. 1997, IAU Circ. 6627
- Turatto, M., et al. 1996, MNRAS, 283, 1

Williams, A. J., et al. 1995, *Rev. Sci. Instrum.*, 66, 2777

Zwicky, F. 1938, *PASP*, 50, 215

Fig. 1.— The R -band light curves of SN 1991T-like, normal, and SN 1991bg-like objects used in the Monte Carlo simulations.

Fig. 2.— The input number distribution of SNe Ia versus apparent magnitude at maximum brightness in the magnitude-limited survey. SNe are binned to an interval of 0.01 mag.

Fig. 3.— The number distribution of discovered SNe Ia versus apparent magnitude at maximum brightness in the magnitude-limited surveys. Only two cases are shown here: SN 1991bg-like objects, and SN 1991T ($A=0$). The upper panel shows the distribution of the peculiar SNe Ia, while the lower panel shows the corresponding distribution of the normal objects. Results for different baselines are shown for each type of SN. The dotted lines labeled “perfect” mark the expected number distributions if all SNe are discovered.

Fig. 4.— The discovery efficiency for the magnitude-limited surveys found in the simulations. The upper panel shows the discovery efficiency for the SN 1991bg-like and the normal objects, the middle panel shows it for the SN 1991T-like and the normal objects, while the lower panel shows it for the SN 1991T-like and the normal objects without considering the age bias. The dashed line is the discovery efficiency for the normal objects for the case SN 1991T ($A=0.4$), and the dotted line for the case SN 1991T ($A=0.8$).

Fig. 5.— The number distribution of SNe versus the epoch of discovery for the magnitude-limited surveys. (Epoch = 0 is defined to be the day of B maximum brightness.) Only two cases are illustrated here: SN 1991bg-like objects, and SN 1991T ($A=0$). The upper panel shows the distribution of the peculiar SNe Ia, while the lower panel shows the corresponding distribution of the normal objects. Results for different baselines are given.

Fig. 6.— The peculiarity rate in the magnitude-limited surveys found in the simulations. The upper panel shows the result for the SN 1991bg-like objects, while the lower panel shows results for the SN 1991T-like objects. The dash-dotted line is the input rate for each type of supernova.

Fig. 7.— The input number distribution of SNe Ia versus apparent magnitude at maximum brightness in the distance-limited surveys. SNe are binned to an interval of 0.01 mag. The dashed line is the number distribution for the case SN 1991T ($A=0.4$) and the dotted line is that for the case SN 1991T ($A=0.8$).

Fig. 8.— The number distribution of discovered SNe Ia versus apparent magnitude at maximum for the distance-limited surveys. Only the case of SN 1991T ($A=0.8$) is shown here for different limiting magnitudes with different baselines. The dotted lines mark the expected number distribution if all SNe are discovered. In the lower two panels they are indistinguishable from the results of the simulations.

Fig. 9.— The discovery efficiency for the distance-limited surveys. The upper panel shows the discovery efficiency for the peculiar SNe Ia, while the lower panel shows the corresponding efficiency for the normal ones.

Fig. 10.— The number distribution of SNe versus the epoch of discovery for the distance-limited surveys. (Epoch = 0 is defined to be the day of B maximum brightness.) Only two cases are shown here: SN 1991bg-like objects, and SN 1991T ($A=0.8$). For each case, results for different baselines are illustrated with different limiting magnitudes.

Fig. 11.— The peculiarity rates in the distance-limited surveys found in the simulations. Results are shown for different baselines and different limiting magnitudes. The solid, dashed, and dash-dotted lines are for the cases of a limiting magnitude of 19.0, 17.0, and 15.0, respectively. The dotted lines are the input rate.

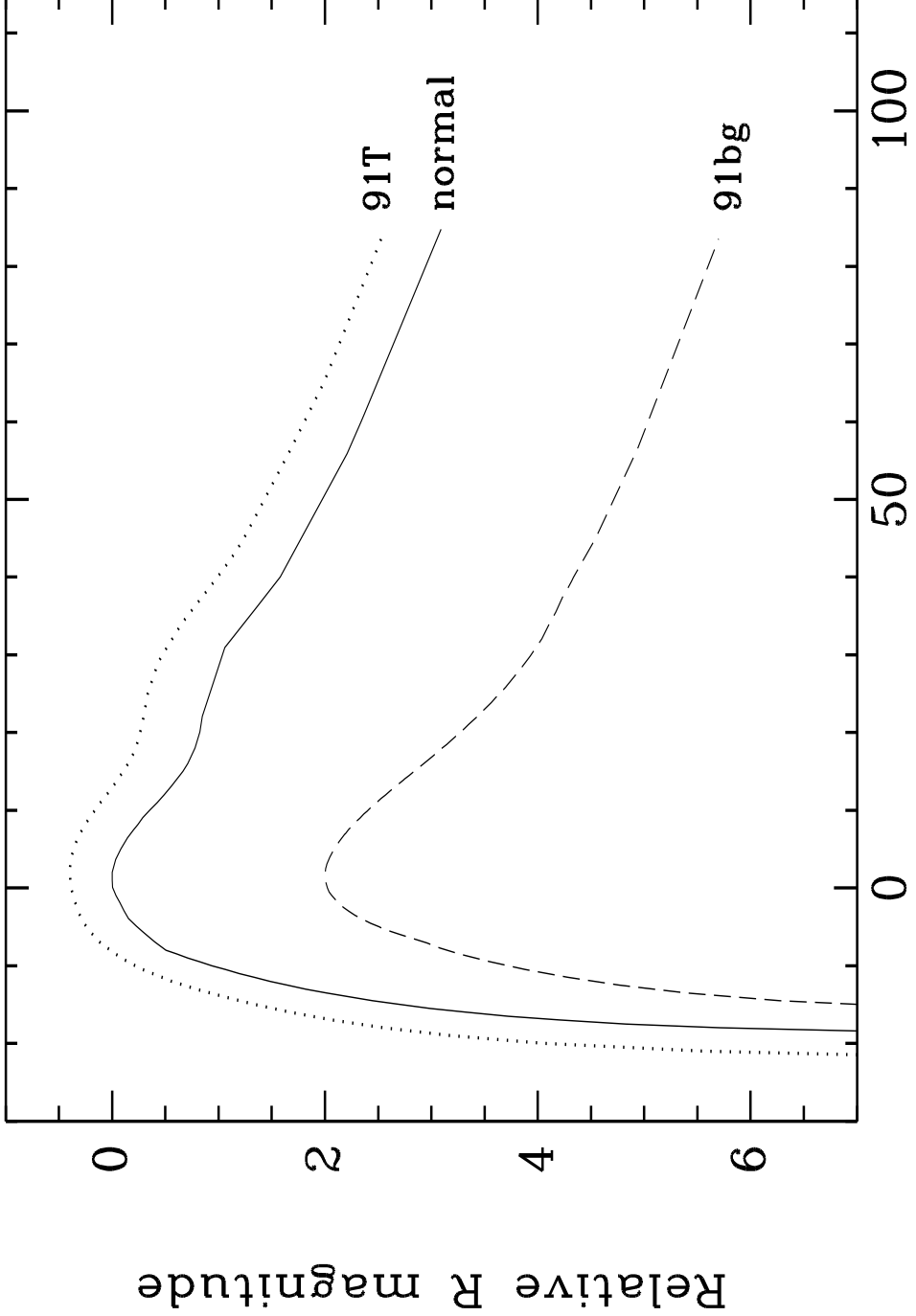
Fig. 12.— The B -band light curves of SN 1991T-like, normal, and SN 1991bg-like objects used in the Monte Carlo simulations.

Fig. 13.— Comparison of the results of the peculiarity rate in the magnitude-limited surveys in the B and R passbands. The upper panel shows the result for the SN 1991bg-like objects, while the lower panel gives results for the SN 1991T-like objects. The dash-dotted line is the input rate for each type of SN. The lines with solid circles are those for the results in the B band, while the others are for those in the R band.

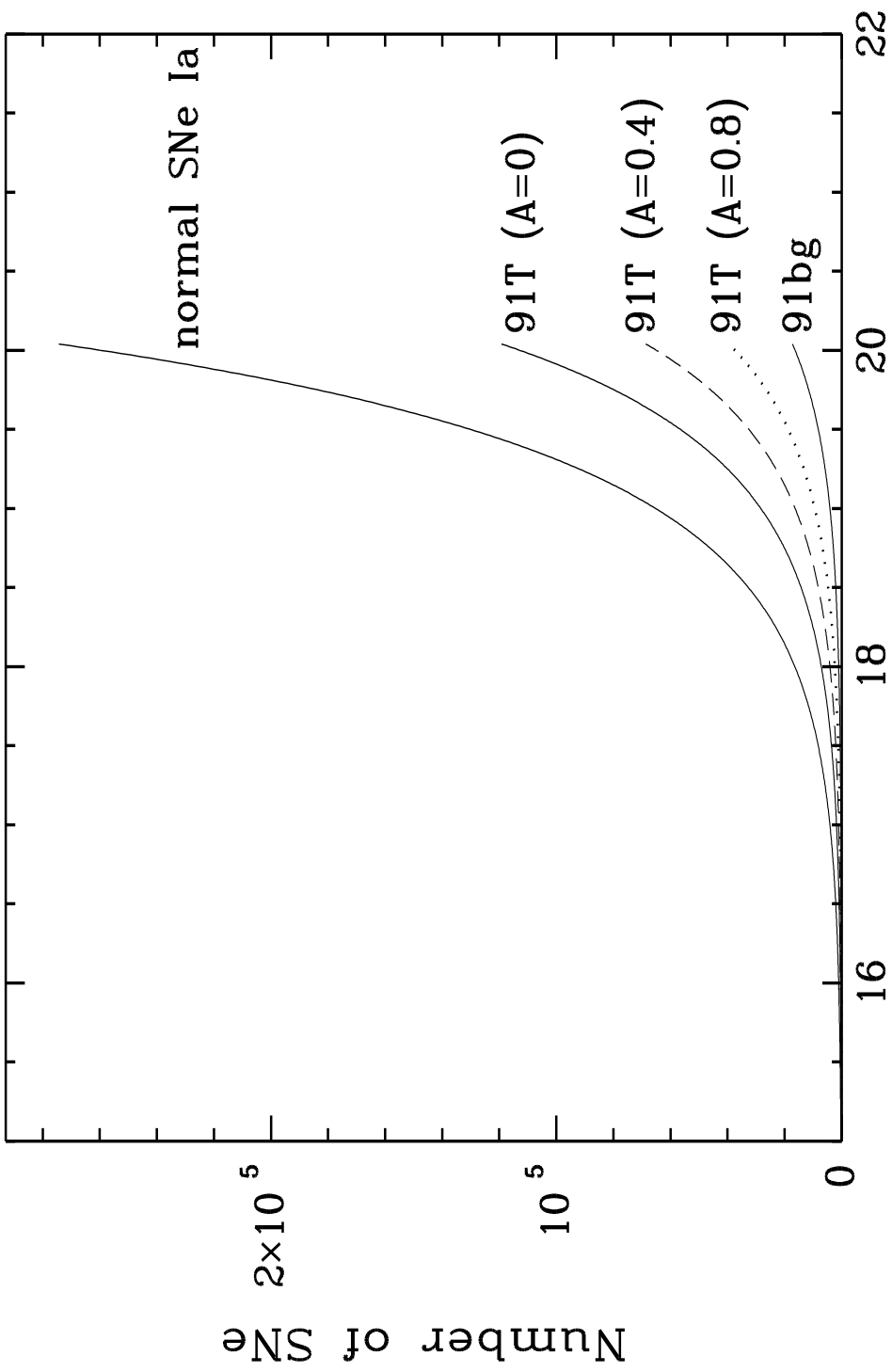
Fig. 14.— The rates of SN 1991T-like objects in the magnitude-limited surveys with different cutoffs for the age bias. In each panel the solid, dashed, and dash-dotted lines are the results for cutoffs of 7, 3, and -1 days past maximum brightness, respectively. The dotted lines are the input rate.

Fig. 15.— The rates of SN 1991T-like objects in the distance-limited SN surveys with different cutoffs for the age bias. From left to right: The limiting magnitude of 19.0, 17.0, and 15.0 cases; from top to bottom: the cases SN 1991T ($A=0$), ($A=0.4$), ($A=0.8$). In each panel the solid, dashed, and dash-dotted lines are the results for a cutoff of 7, 3, and -1 day past maximum brightness for the age bias, respectively. The dotted lines are the input rate.

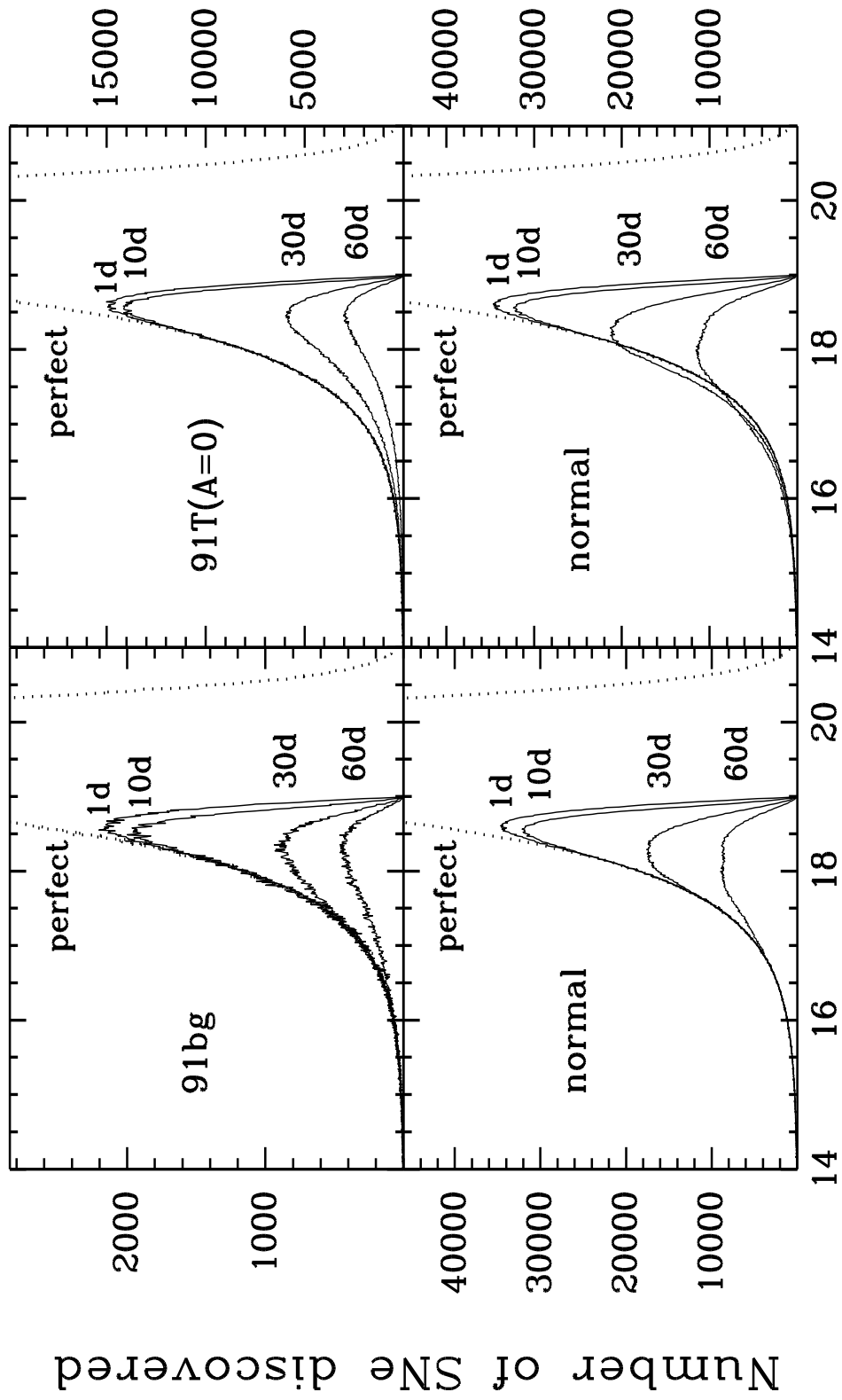
Fig. 16.— Comparison of the distribution of the epoch of discovery from the simulations with that from LOSS+BAOSS and CTSS. The upper panel shows the results from CTSS (*solid line*) and a magnitude-limited survey with a baseline of 20 days (*dashed line*), while the lower panel shows those from LOSS+BAOSS (*solid line*) and a distance-limited survey with a baseline of 10 days and a limiting magnitude of 19.0.



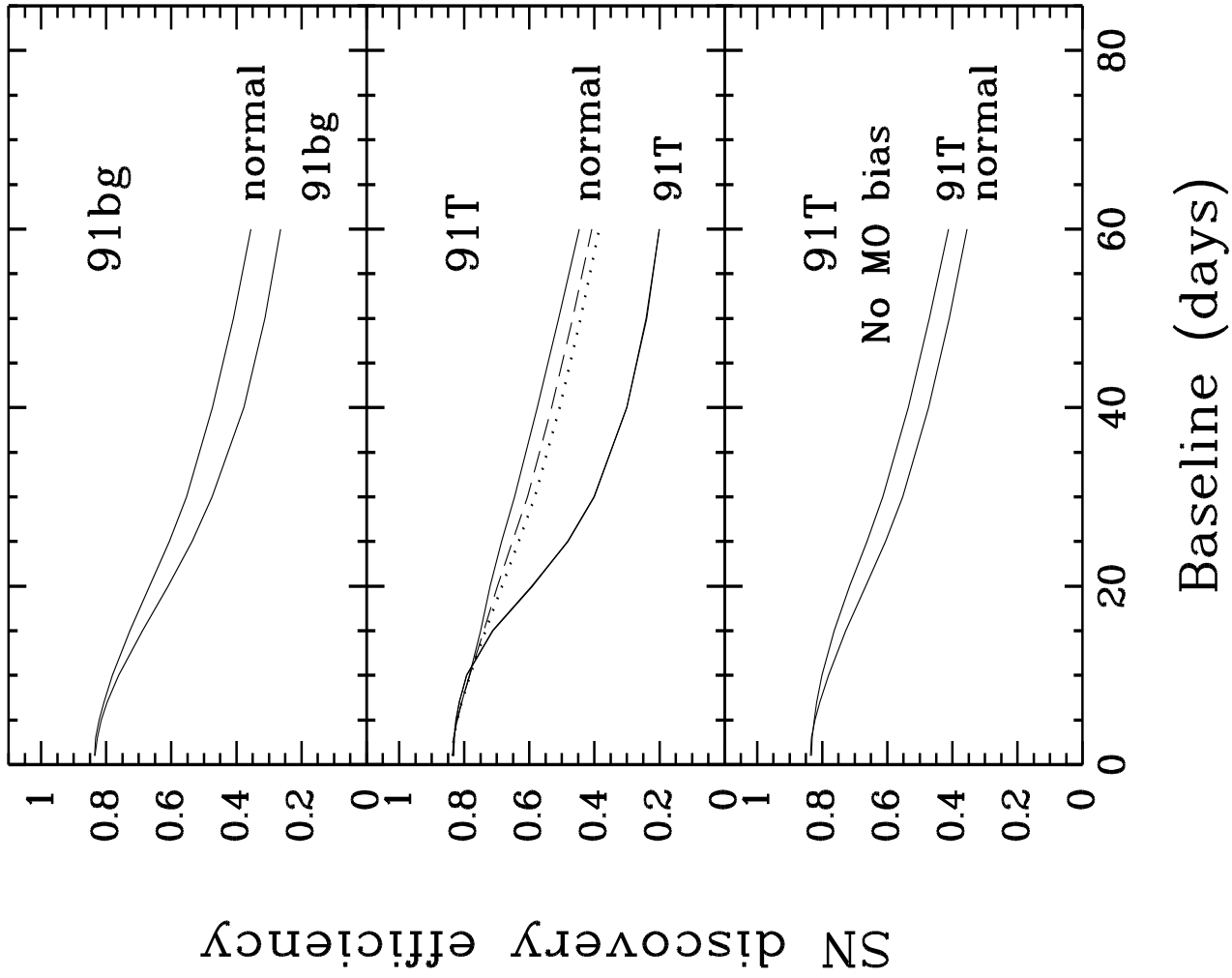
Days after maximum brightness

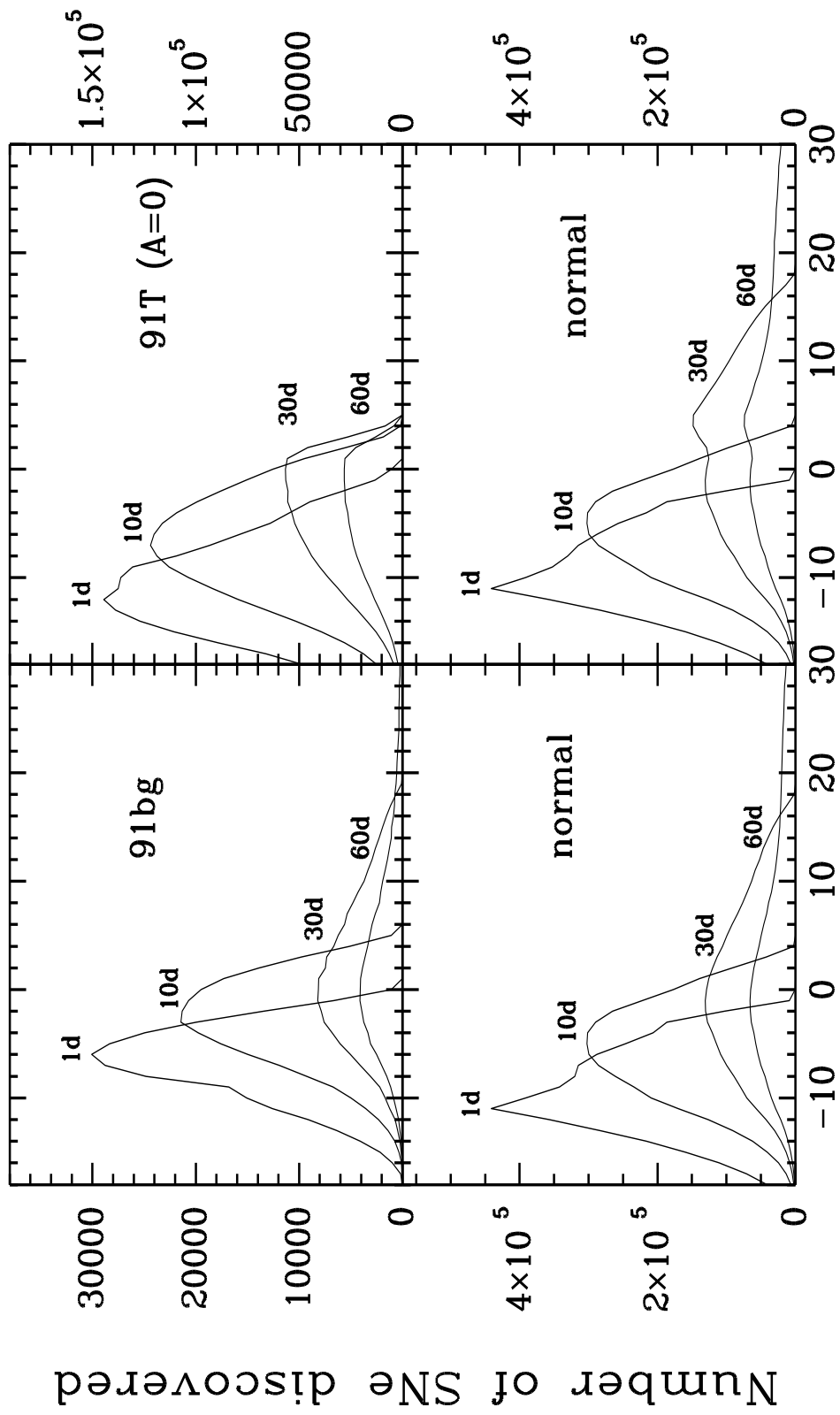


Apparent magnitude at maximum brightness

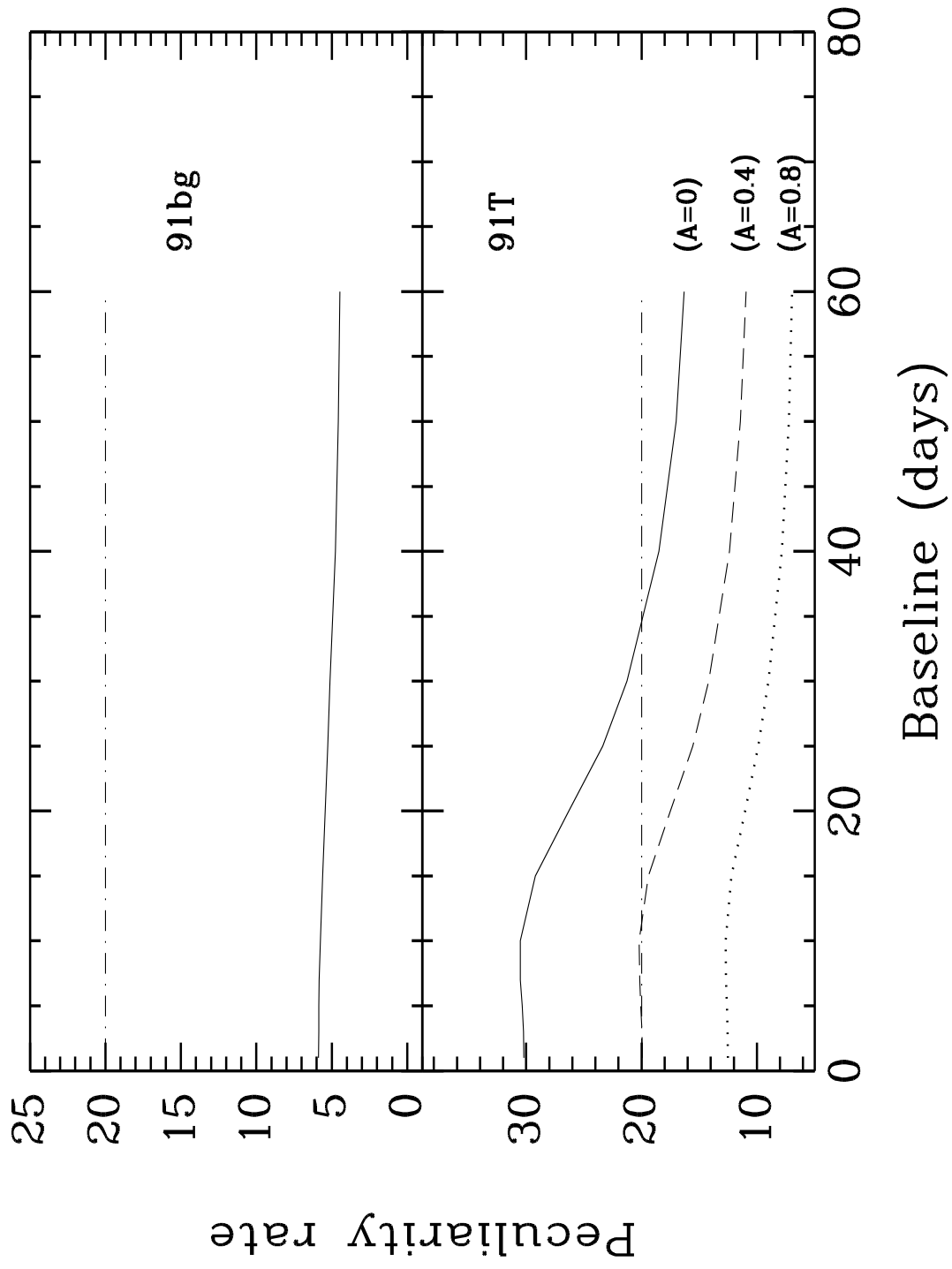


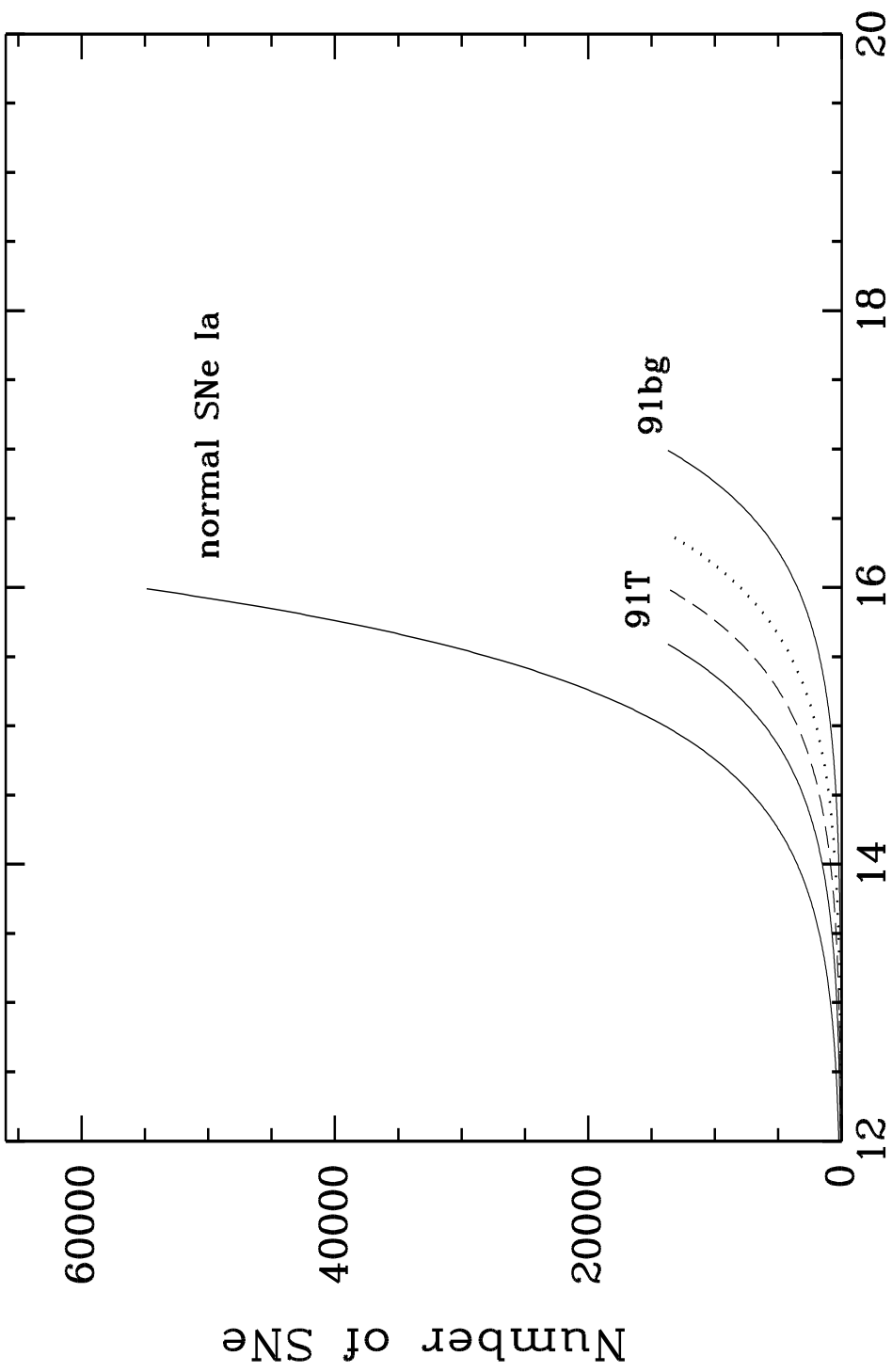
Apparent magnitude at maximum brightness



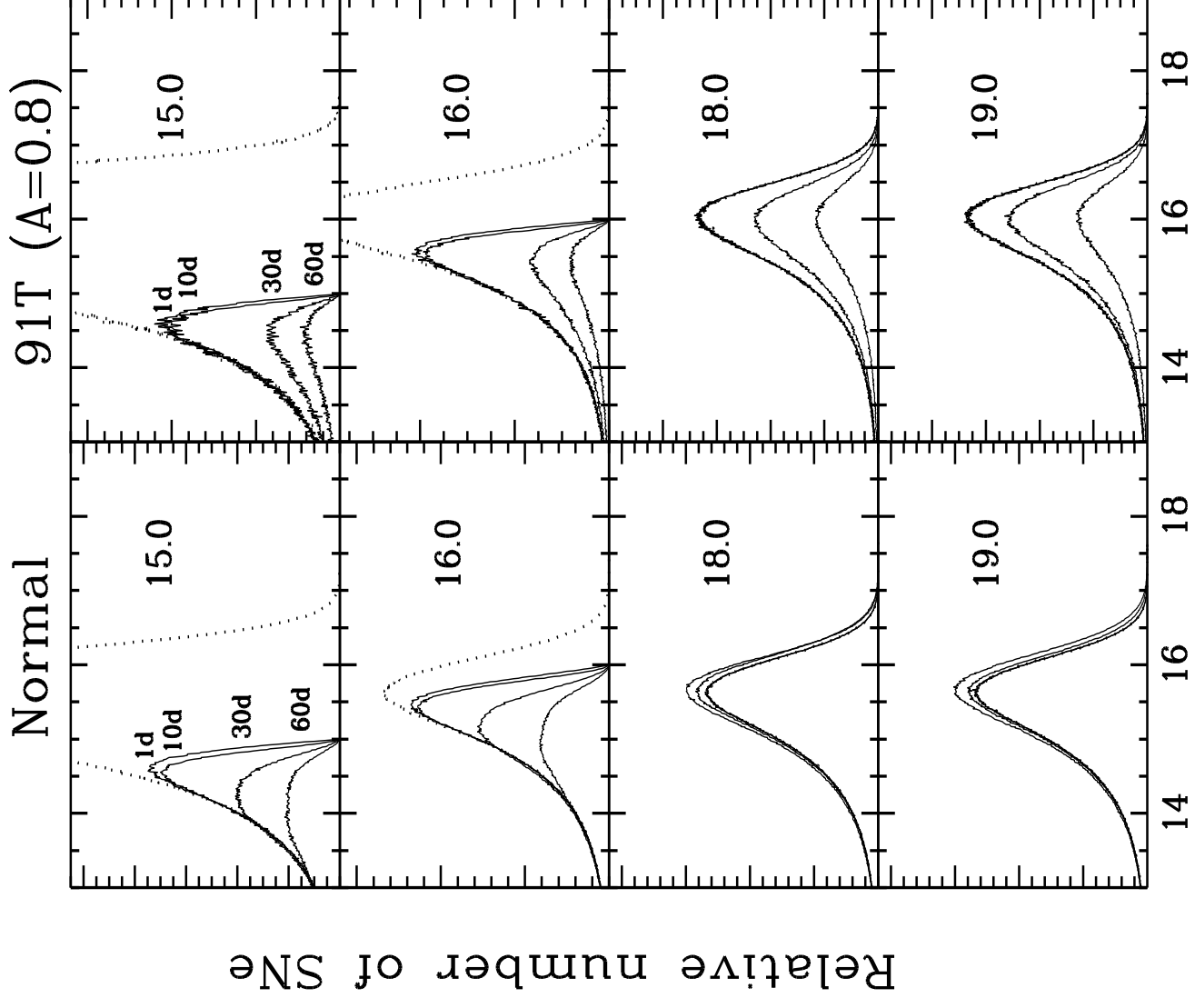


Discovery epoch (0 = maximum brightness)

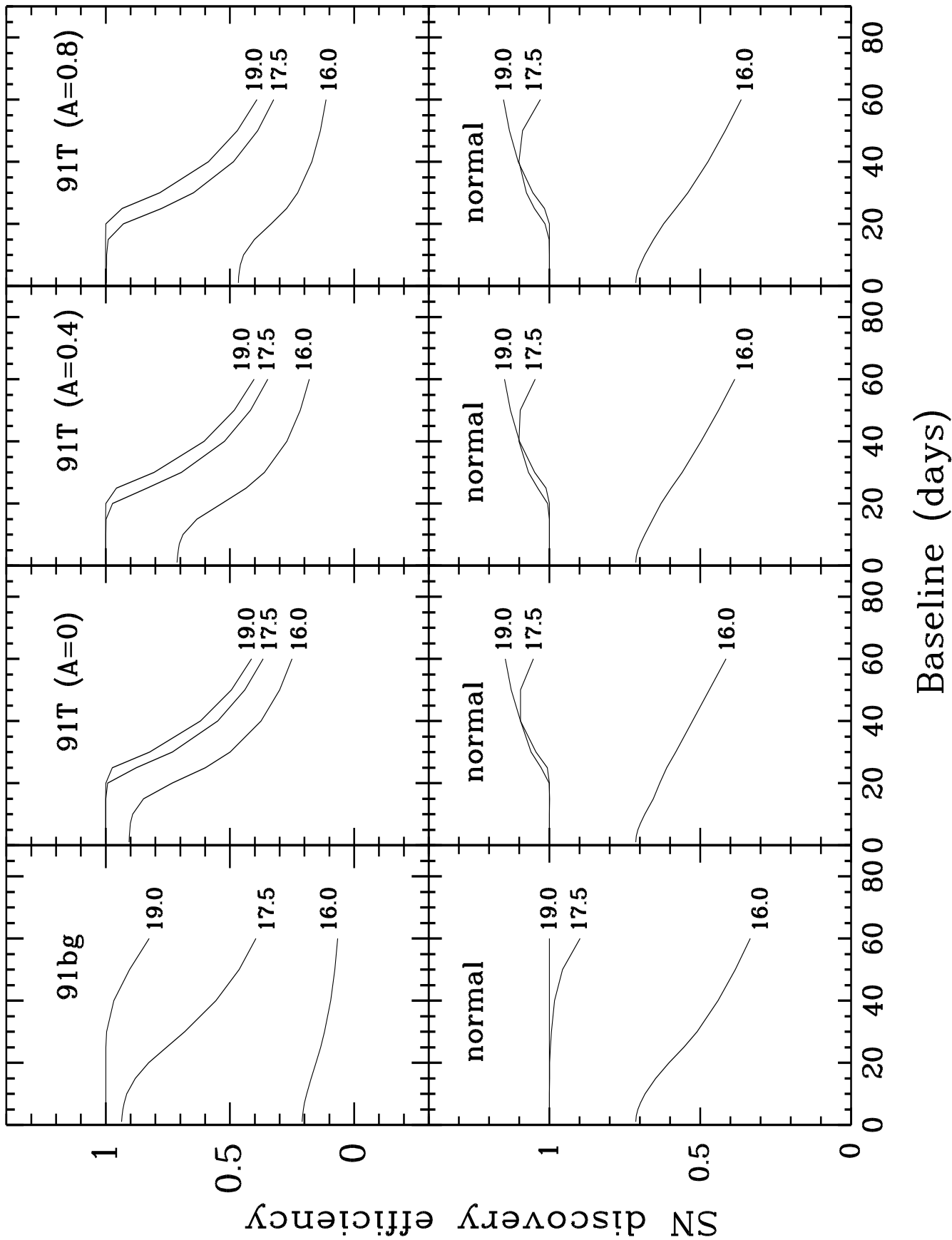




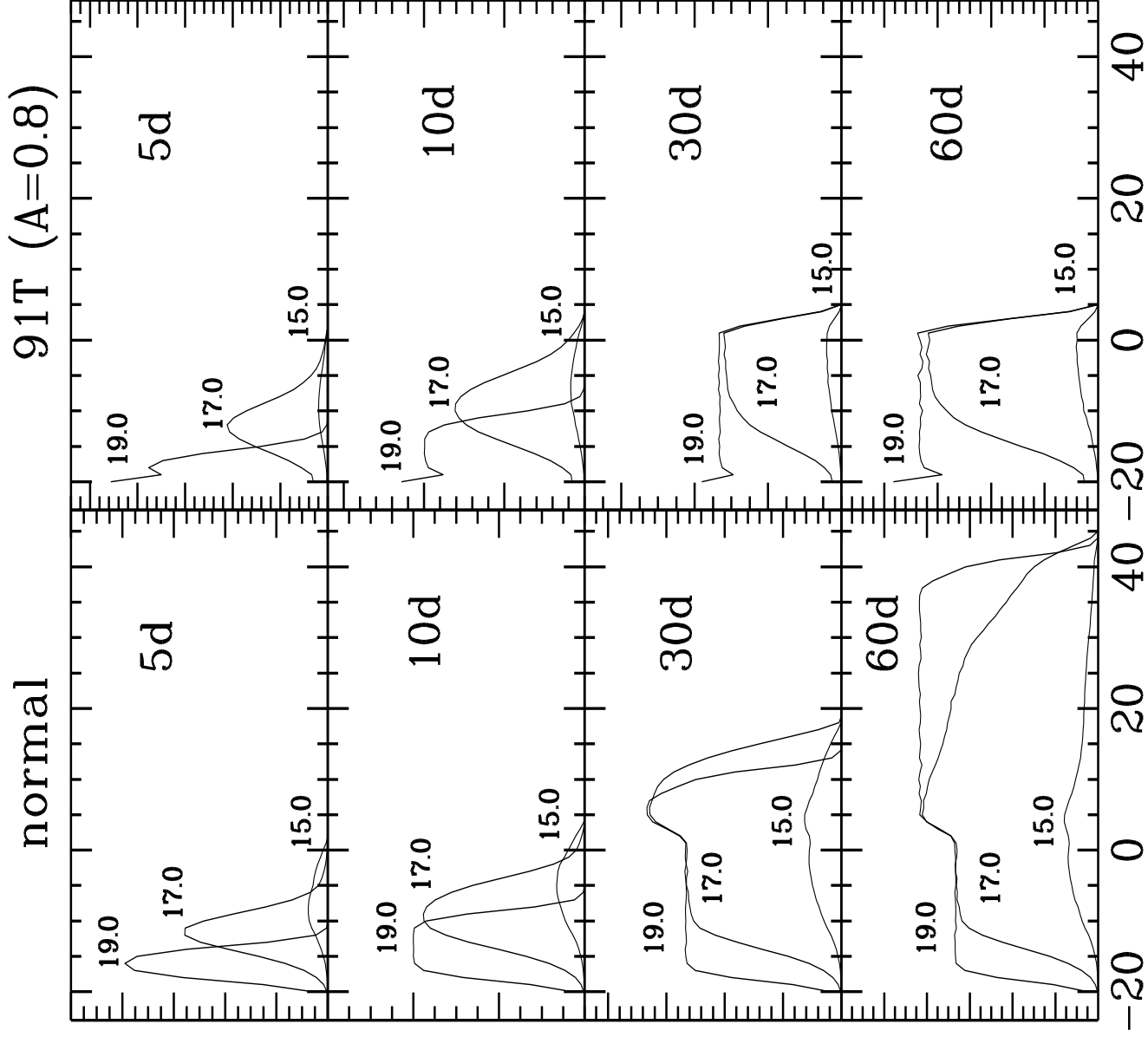
Apparent magnitude at maximum brightness



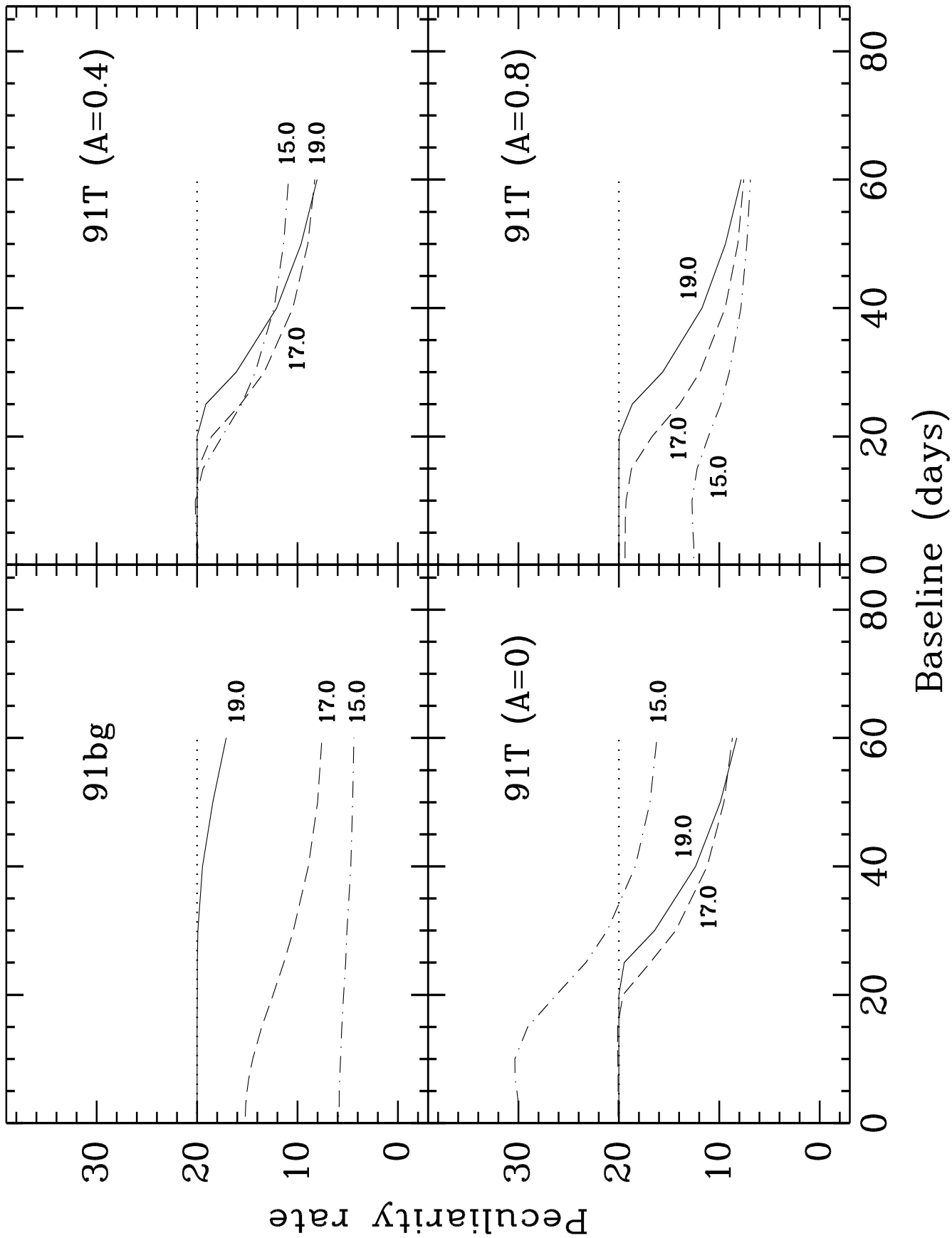
Apparent magnitude at maximum brightness

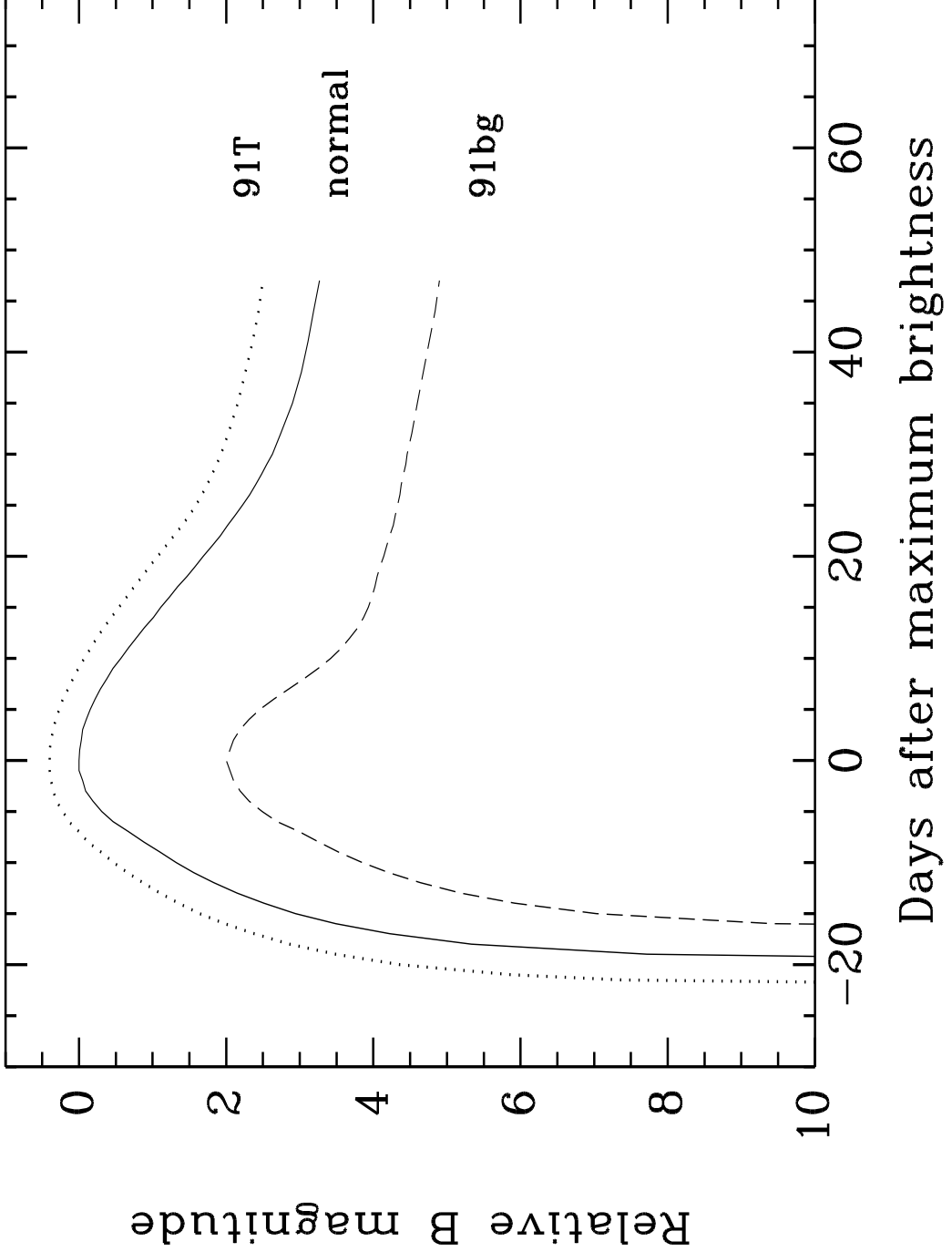


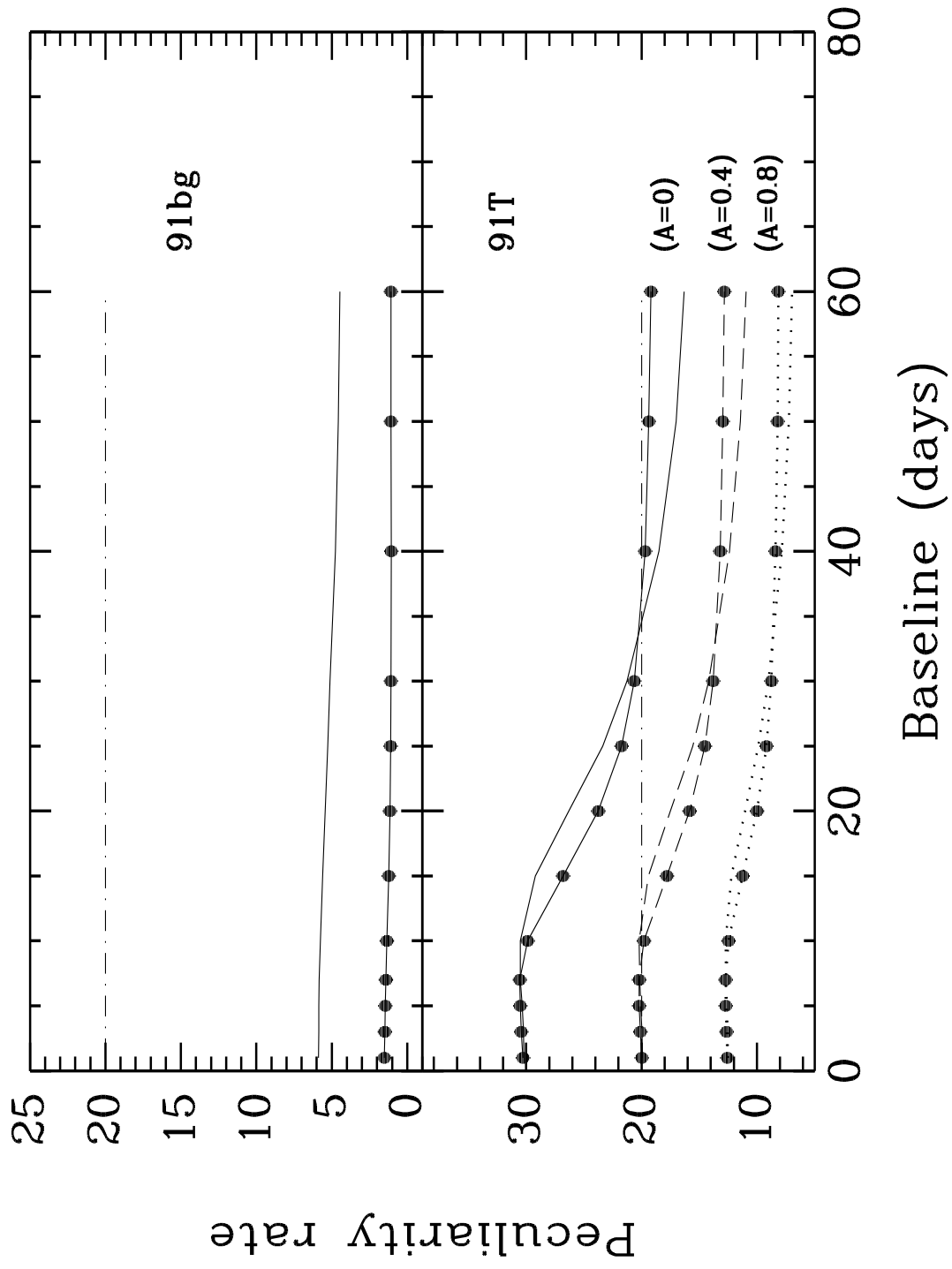
Relative number of SNe

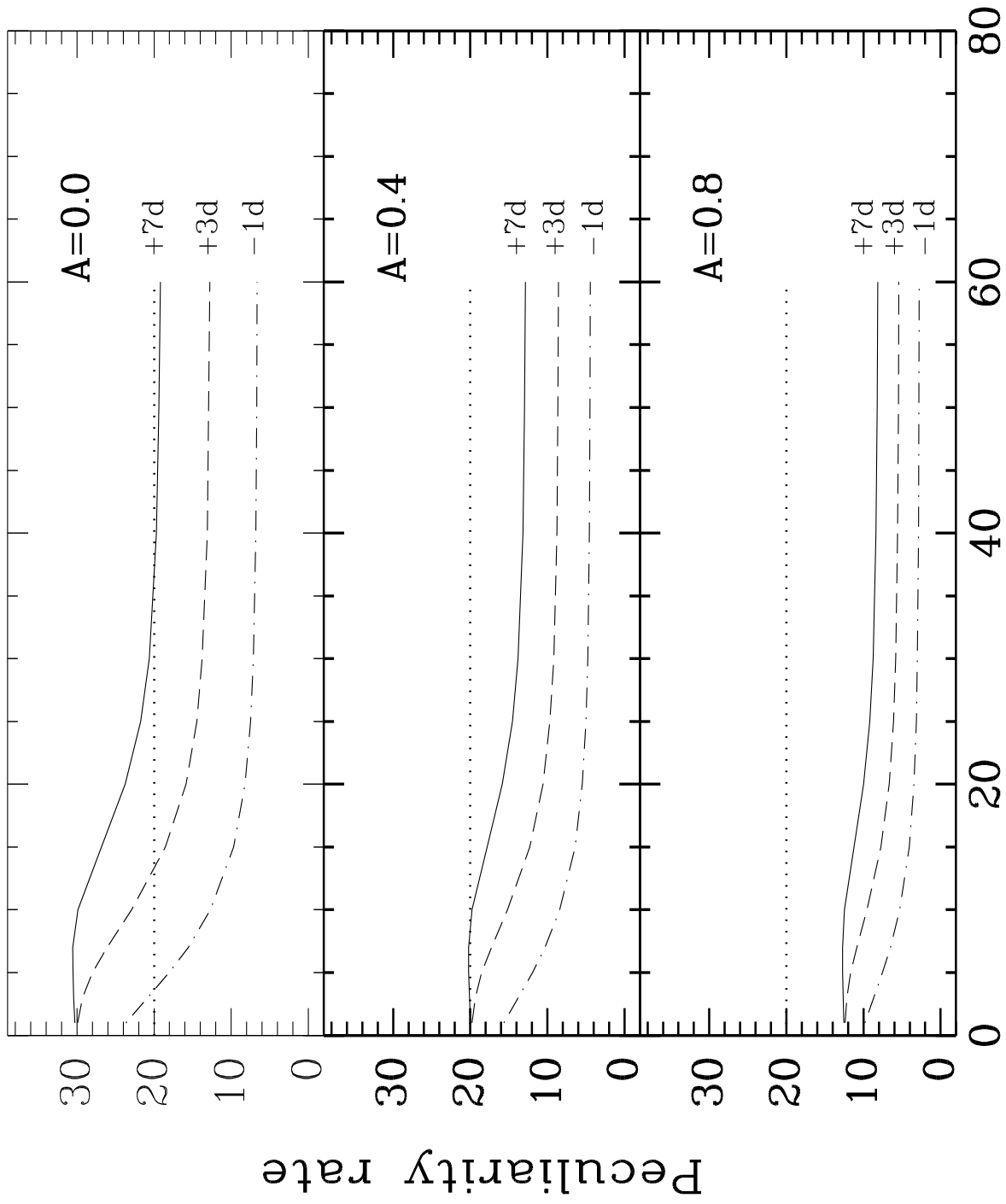


Discovery epoch (0 = maximum brightness)









Baseline

